

# Exciton Polaritons in Emergent Two-Dimensional Semiconductors

Haifeng Kang, Jingwen Ma,\* Junyu Li, Xiang Zhang,\* and Xiaoze Liu\*



Cite This: *ACS Nano* 2023, 17, 24449–24467



Read Online

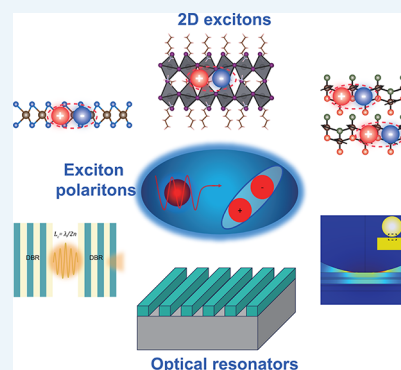
ACCESS |

Metrics & More

Article Recommendations

**ABSTRACT:** The “marriage” of light (i.e., photon) and matter (i.e., exciton) in semiconductors leads to the formation of hybrid quasiparticles called exciton polaritons with fascinating quantum phenomena such as Bose–Einstein condensation (BEC) and photon blockade. The research of exciton polaritons has been evolving into an era with emergent two-dimensional (2D) semiconductors and photonic structures for their tremendous potential to break the current limitations of quantum fundamental study and photonic applications. In this Perspective, the basic concepts of 2D excitons, optical resonators, and the strong coupling regime are introduced. The research progress of exciton polaritons is reviewed, and important discoveries (especially the recent ones of 2D exciton polaritons) are highlighted. Subsequently, the emergent 2D exciton polaritons are discussed in detail, ranging from the realization of the strong coupling regime in various photonic systems to the discoveries of attractive phenomena with interesting physics and extensive applications. Moreover, emerging 2D semiconductors, such as 2D perovskites (2DPK) and 2D antiferromagnetic (AFM) semiconductors, are surveyed for the manipulation of exciton polaritons with distinct control degrees of freedom (DOFs). Finally, the outlook on the 2D exciton polaritons and their nonlinear interactions is presented with our initial numerical simulations. This Perspective not only aims to provide an in-depth overview of the latest fundamental findings in 2D exciton polaritons but also attempts to serve as a valuable resource to prospect explorations of quantum optics and topological photonic applications.

**KEYWORDS:** 2D semiconductors, strong coupling, exciton polaritons, transition metal dichalcogenides (TMDs), topological photonics, nonlinear interactions, valley degree of freedom, Bose–Einstein condensation



Exciton-polaritons are hybrid quasiparticles arising from the strong coupling between resonant excitons and photons, where the energy exchange rate exceeds the average decay rates of the excitons and photons.<sup>1,2</sup> In the strong coupling regime, exciton polaritons feature splitting of resonance energy, exhibiting a distinct hybrid nature by leveraging advantageous characteristics of the exciton and photon constituents<sup>2–7</sup> (Figure 1a). On the one hand, the exciton constituent in semiconductors provides spin sensitivity, electrical tunability, and strong bosonic interactions as underlying mechanisms for nonlinear optics and quantum phenomena.<sup>2–9</sup> On the other hand, the photon constituent, typically confined within optical resonators, gives rise to small effective mass, spatial coherence and versatile optical degrees of freedom (DOFs) for photonic behaviors such as absorption, reflection, photoluminescence (PL), scattering, propagation, etc.<sup>2–7,10–15</sup> These hybrid characteristics result in intriguing quantum phenomena such as Bose–Einstein condensation (BEC),<sup>2,16–18</sup> superfluidity,<sup>19–22</sup> quantum blockade,<sup>23–32</sup> topological flows,<sup>33–35</sup> etc., leading to the rapid research progresses of exciton polaritonics. The basic physical concepts

for the exciton and photon constituents as well as the underlying mechanisms for the strong coupling are elaborated as following.

## EXCITONS IN SEMICONDUCTORS

Excitons are electron–hole pairs bound by Coulomb interactions in semiconductors.<sup>36</sup> These electron–hole pairs are regarded as electrical dipoles that could interact with the optical field.<sup>36–39</sup> This interaction can be described in terms of oscillator strength  $f$ :<sup>36–39</sup>

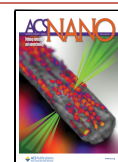
$$f = \frac{2m^*\omega}{\hbar} |\langle \mu_h | r \cdot e | \mu_e \rangle|^2 \frac{V_{ex}}{\pi d_B^3} \quad (1)$$

**Received:** August 24, 2023

**Revised:** November 22, 2023

**Accepted:** November 28, 2023

**Published:** December 5, 2023



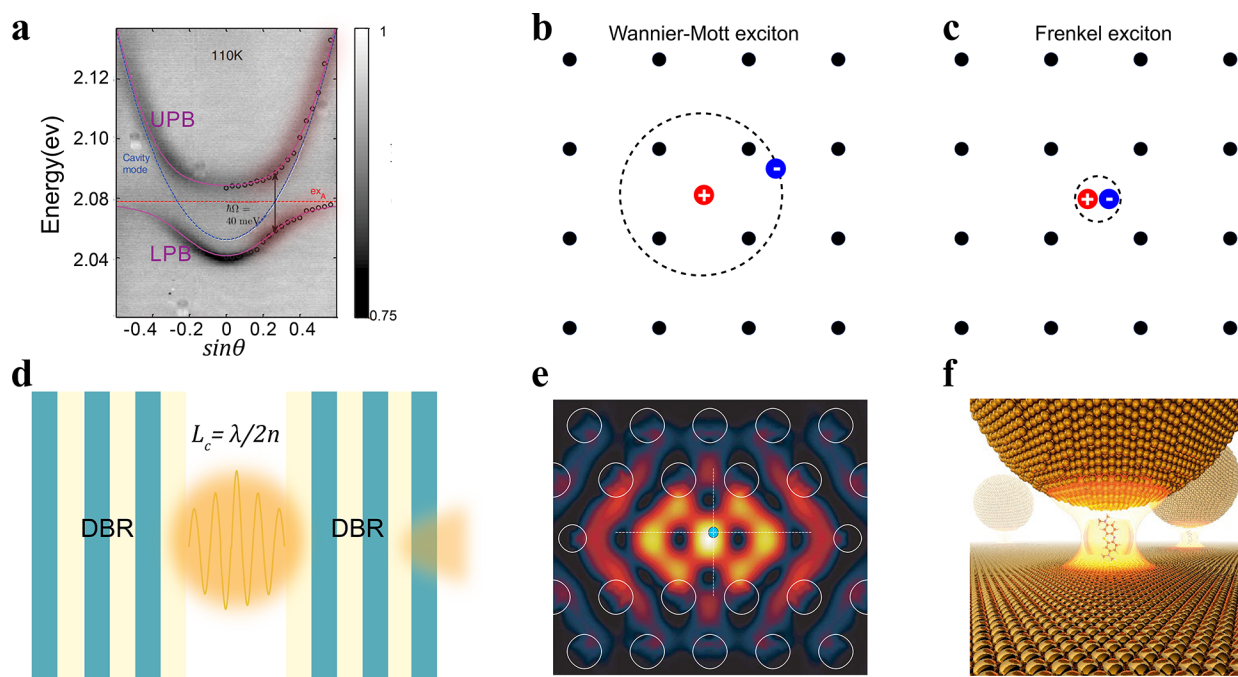


**Figure 1.** Fundamental concepts for semiconductor excitons, optical resonators, and exciton polaritons. (a) Angle-resolved dispersion of 2D exciton polariton, where UPB and LPB represent the upper and lower polariton branches, respectively,  $\hbar\Omega$  represents the Rabi splitting. The blue curve represents the cavity mode, and the red-dashed line represents the exciton state. The red clouds in the polariton dispersion highlight the bending of the dispersion at large angles. Schematics of (b) Wannier–Mott excitons and (c) Frenkel excitons. (d) Schematic of a Fabry–Pérot (FP) microcavity, consisting of two mirrors and a cavity layer, whose optical length ( $L_c$ ) is integer number of half wavelength ( $\lambda$ ). The mirrors could be DBR or a thin metal film. (e) Schematics of the photonic crystal cavity. (f) Schematic of a plasmonic nanocavity (NPoM). Panel (a) reprinted with permission from ref 86. Copyright 2017 American Physical Society. Panel (e) reprinted with permission from ref 87. Copyright 2007 Springer Nature. Panel (f) reprinted with permission from ref 62. Copyright 2016 Springer Nature.

where  $m^*$  represents the effective mass of the excitons,  $|\mu_c\rangle$  and  $|\mu_h\rangle$  are Bloch wave functions of electrons and holes,  $V_{ex}$  is the interaction volume between exciton and light,  $a_B$  is the Bohr radius of exciton. The larger the oscillator strength, the stronger the interaction between excitons and photons emerges.

Two of the most common excitons are Wannier–Mott excitons and Frenkel excitons, each of which possesses distinctive physical properties.<sup>37,40–42</sup> In Wannier–Mott excitons,<sup>37,40,42</sup> commonly observed in inorganic semiconductors, the electron and hole are spatially separated and located at different lattice sites (Figure 1b). The exciton Bohr radius is larger than the lattice constants for delocalized electron–hole pairs, resulting in relatively small oscillator strengths and weak binding energies (typically ranging from a few to 100 meV). In most cases, the Wannier–Mott excitons can be described by hydrogen-like model with higher excited states of Rydberg series.<sup>37,40,42</sup> But these excited states can only be observed in a few examples for the relatively weak binding energies and finite line widths. In Frenkel excitons,<sup>37,40,41</sup> as found in organic semiconductors, the electron and hole are tightly bound at different molecular orbitals but reside within the same molecules (Figure 1c). The exciton Bohr radius is small for localized electron–hole pairs, resulting in a large oscillator strength and strong binding energies (typically around a few hundreds of meV). The Frenkel excitons cannot be well described by the hydrogen models, but are generally analyzed based on electronic transitions between different molecular orbitals.<sup>37,40,41</sup>

There emerge distinct excitons in two-dimensional (2D) semiconductors that cannot simply be understood by the

above-mentioned models of Wannier–Mott excitons and Frenkel excitons.<sup>38,39,43–51</sup> On the one hand, 2D excitons possess large oscillator strength and strong binding energy<sup>38,39,44,47–50,52–55</sup> which are comparable with Frenkel excitons, due to the quantum confinements and dielectric screening. On the other hand, the electron–hole pairs are not so localized that they span over several crystalline lattice sites, which are still in the framework of the Wannier–Mott exciton model but with some modification.<sup>38,39,44,47–50,52–55</sup> These attractive properties of 2D excitons present numerous exciting opportunities to investigate fascinating light–matter interactions, supporting fantastic avenues for investigating the exciton polaritons for fundamental quantum research and optoelectronic applications.<sup>5,6,8,56–60</sup> Typical semiconductor examples for 2D excitons are van der Waals semiconductors, including monolayer transition metal dichalcogenides (TMDs), 2D perovskites (2DPKs), and 2D antiferromagnetic (AFM) semiconductors, which will be discussed in more detail later.

**Photons Confined in Optical Resonators.** Confined photons are another indispensable constituent for the strong coupling of exciton polaritons, which are characterized by two critical parameters of optical resonators, i.e., quality factor and mode volume.<sup>61,62</sup> The quality factor  $Q = \omega/\delta\omega$ , where  $\omega$  and  $\delta\omega$  present resonant frequency and frequency line width of confined photons, represents the number of cycles that photons are trapped in an optical resonator before the photons' leakage.<sup>61,62</sup> The mode volume  $V = \int_V \epsilon(r)|E^2(r)| d\Omega/\max\{E^2\}$ , where  $\epsilon(r)$  and  $E(r)$  are the dielectric function and electric field distribution inside the optical resonator, respectively, exhibits the spatial volume in which photons are confined.<sup>61,62</sup> Based on these definitions, the quality factor and

mode volume of optical resonators represent the confinements of photons in the time and space dimensions, respectively. The spectral range of interests in this Perspective is at the visible and near-infrared (400 nm–1.7  $\mu\text{m}$ ), if no additional information is specified. In this context, three main types of optical resonators are discussed in terms of quality factor and mode volume: Fabry-Pérot (FP) microcavities, photonic crystals (PC), and plasmonic nanocavities.

The FP microcavities, typically composed of two facing mirrors of high reflectance and a cavity layer (Figure 1d), are the most straightforward resonators and the most widely used ones. FP cavities typically have high quality factors, which are proportional to the reflectance of the mirror materials. For mirrors of near-unity reflectance, the quality factor can reach  $Q \sim 10^5$  in the near-infrared spectrum.<sup>61,63</sup> and the typical mode volume largely exceeds the wavelength volume ( $V > (\lambda/n)^3$ ),<sup>61,62</sup> where  $n$  is the refractive index of the media. The high reflectance can be realized by distributed Bragg reflectors (DBR), which are the most chosen option for the mirrors of FP cavities. DBR refer to one-dimensional photonic crystals of alternate dielectric layers with contrasting refractive indices, whose optical lengths are designed to be a quarter of a specific wavelength.<sup>2</sup> At this wavelength, each dielectric layer can support destructive interference, and several periods of such interfering layers can result in near-unity reflectance with finite bandwidths. Grating structures and noble metallic films can also support considerably high reflectance for the top mirrors (from which photons can leak out). The cavity layer determines the photon modes of FP cavities by its optical length, and the photon energy can be described by a  $L_c$  cavity length as<sup>2</sup>

$$E_{\text{ph}} = \frac{\hbar c}{n} \sqrt{k_{\parallel}^2 + \left(\frac{\pi m}{L_c}\right)^2} \quad (2)$$

where  $k_{\parallel}^2 = k_x^2 + k_y^2 = \frac{2\pi}{\lambda_c} \tan(\theta)$  represents the in-plane wave-number,  $\theta$  is the incidence angle,  $\lambda_c$  is the cavity resonance wavelength at normal incidence,  $n$  is refractive index of the cavity layer,  $m$  is an integer number. With translation invariance, the cavity mode can be characterized by angle-resolved spectroscopy, where the angle ( $\theta$ ) shares a one-to-one correspondence with the in-plane wavenumber.

The PC cavities, typically composed of periodic nanostructures of dielectric materials, can support confined photons via the photonic band structures. The quality factor  $Q$  of PC generally could be notably high, some of which can easily get over  $10^4$  and even reach above  $10^6$ .<sup>61,64</sup> On the other hand, the mode volume approximate to  $(\lambda/n)^3$  (the scale from  $\mu\text{m}^3$  to  $\text{nm}^3$  depending on the specific nanostructures and the photonic modes<sup>61,64</sup>). PC cavities can be either one-dimensional (1D) or two-dimensional (2D), depending on their dimensions of periodicity. The simplest form of PC structure entails 1D optical gratings, wherein resonant performance hinges on various geometric attributes like filling factor, period, and dielectric thickness.<sup>64–66</sup> The 1D PC can provide efficient light manipulation only along the direction of periodicity. Upgrading the PC nanostructures to 2D lattices introduces additional degrees of freedom to manipulate the photons at nanoscales. Typical 2D PC can be fabricated as periodic nanoholes, nanopillars, etc.<sup>64,67–69</sup> In PC nanostructures, high  $Q$  photonic resonances emerge either from the edge of certain photonic bands, or from carefully engineered defect structures

breaking the periodic of PCs.<sup>64–69</sup> Compared with conventional FP cavities, the rich photonic band structures in PCs can lead to various intriguing phenomena. For instance, PC structures can exhibit nontrivial topological behaviors similar to those originally discovered in condensed-matter systems, which have recently emerged as a fascinating platform to manipulate the confined photons protected from photonic defects,<sup>11,12</sup> and lead to the research surge of topological exciton polaritons.<sup>10,15,33–35,70–75</sup> Another very interesting example is PCs exhibiting bound states in continuous (BIC) resonances. These distinct resonances can support ultrahigh  $Q$  resonances bounded to the dielectric slabs even when it is within the continuum bands of lossy radiative modes. Fundamentally, this BIC phenomenon also originates from topological charges in the momentum space, which topologically protect the BIC modes from coupling to lossy radiative modes. All these captivating phenomena in PC nanostructures,<sup>10,15,33–35,70–75</sup> especially when they are strongly coupled to excitons, will be discussed in more details in later context.

Plasmonic nanocavities are usually known to be capable of trapping photons within extremely small mode volume by leveraging the highly confined electromagnetic fields of plasmonic resonances.<sup>62,76–78</sup> The mode volume (generally  $V \ll (\lambda/n)^3$ ) could even reach the size of picometers,<sup>79,80</sup> while the quality factor is small (typically  $Q < 100$ ).<sup>62,76–78</sup> For the extremely small  $V$  and quite small  $Q$ , plasmonic nanocavities on the one hand could significantly facilitate light-matter interactions with enormous field enhancement, on the other hand could be very lossy for photonic applications.<sup>62,76–78</sup> There are various configurations for the plasmonic nanocavities, such as plasmonic arrays (plasmonic crystals)<sup>81–83</sup> and gap plasmons.<sup>62,76–78</sup> The plasmonic arrays are similar to PC, but the unit cells are based on plasmonic nanostructures. The gap plasmons exhibit complex optical modes strongly depending on the dielectric environment, gap size, and nanostructure geometry.<sup>62,76–78</sup> Typical geometries include dimers, bowties, and nanoparticle-on-mirror (NPOM) configurations. Taking the NPOM as an example (Figure 1f), optical modes can be highly confined at the small nanogap between the metallic nanoparticle and the mirror.<sup>62,76–78</sup> More specifically, the optical modes can be described by a resistor-inductor-capacitor (RLC) circuit model. In the NPOM structure, the nanoparticles and substrates are both considered as capacitors and inductors in series, and the sample in the middle is treated as a capacitor; all of these elements have finite impedances. The solution to this RLC circuit yields the resonant modes of the nanocavity.<sup>62,76–78</sup>

**Exciton Polaritons in the Strong Coupling Regime.** As appropriate semiconductors and corresponding optical resonators are integrated together, excitons and photons can couple with each other in the way of energy exchange between them. The Hamiltonian of such coupled system can be written as follows:<sup>2,84</sup>

$$H = \begin{pmatrix} \hbar\omega_{\text{ex}} - i\gamma_{\text{ex}} & g \\ g & \hbar\omega_{\text{ph}} - i\gamma_{\text{ph}} \end{pmatrix} \quad (3)$$

here  $\hbar\omega_{\text{ex}}$  and  $\hbar\omega_{\text{ph}}$  represent the energy of excitons and photons, respectively,  $\gamma_{\text{ex}}$  and  $\gamma_{\text{ph}}$  are the line widths of excitons and cavity photons, respectively. The  $\gamma_{\text{ex}}$  is determined from the intrinsic nature of excitons (i.e., radiative and nonradiative decay rates), while  $\gamma_{\text{ph}}$  is determined from the quality factor  $Q$ .

Moreover,  $g$  is the coupling strength between excitons and photons as  $g \propto \sqrt{f/V}$ , where  $V$  is the mode volume,  $f$  is the oscillator strength of excitons as discussed above.

The eigenvalues of the coupled system Hamiltonian are obtained as<sup>2,84</sup>

$$\omega_{\pm} = \frac{\omega_{\text{ex}} + \omega_{\text{ph}}}{2} - i \frac{\gamma_{\text{ex}} + \gamma_{\text{ph}}}{2} \pm \sqrt{g^2 + (\omega_{\text{ph}} - \omega_{\text{ex}} - i(\gamma_{\text{ph}} - \gamma_{\text{ex}}))^2} \quad (4)$$

For these two eigenvalues, when excitons and photons are in resonance (i.e., the detuning ( $\delta = \omega_{\text{ph}} - \omega_{\text{ex}}$ ) is equal to zero), the difference between them is termed as “Rabi splitting”:

$$\Omega_{\text{R}} = \sqrt{4g^2 - (\gamma_{\text{ph}} - \gamma_{\text{ex}})^2} \quad (5)$$

This Rabi splitting could bring up energy level splitting of the two eigenvalues when  $g > |\gamma_{\text{ph}} - \gamma_{\text{ex}}|/2$ . Note the split energy levels here does not necessarily mean the photonic system reaches the strong coupling yet. Only when  $g > \sqrt{(\gamma_{\text{ph}}^2 + \gamma_{\text{ex}}^2)}/2$ , the strong coupling regime is reached that the higher one of the eigenvalues is called as the upper polariton and the lower one as the lower polariton.<sup>2,6,84,85</sup> Moreover, the photonic system may refer to the intermediate coupling regime when  $|\gamma_{\text{ph}} - \gamma_{\text{ex}}|/2 < g < \sqrt{(\gamma_{\text{ph}}^2 + \gamma_{\text{ex}}^2)}/2$ .<sup>2,6,84,85</sup>

In the strong coupling regime, Hopfield coefficients are defined as<sup>2,6,84,85</sup>

$$X^2 = \frac{1}{2} \left( 1 + \frac{\delta}{\sqrt{\delta^2 + 4g^2}} \right) \quad (6)$$

$$C^2 = \frac{1}{2} \left( 1 - \frac{\delta}{\sqrt{\delta^2 + 4g^2}} \right) \quad (7)$$

where  $X^2 + C^2 = 1$ . The Hopfield coefficients of  $X^2$  and  $C^2$  represent the fractions of excitons and photons in the strongly coupled exciton polaritons, respectively. The Hopfield coefficients are a critical measure for the hybrid nature of exciton polaritons so that they could leverage advantages from both exciton and photon constituents. When  $X^2$  is larger and close to unity, exciton polaritons become more exciton-like with more excitonic properties; when  $C^2$  is approaching unity, on the other hand, exciton polaritons become more photon-like with specific photonic properties from optical resonators.

**Hallmarks for the Research Progresses of Exciton Polaritons.** It has been more than three decades since the observation of exciton polaritons in quantum wells embedded in a FP cavity.<sup>1</sup> Throughout these decades, exciting progress has been made, vigorously propelling the quantum research of exciton polaritons forward, as sketched in the two intertwining timelines of Figure 2. One of the timelines marks the significant achievements with more emphasis on the excitonic research, while the other highlights the critical accomplishments mostly enabled by the photonic properties. Although the research progresses are marked in these two ways, they are actually quite dependent on each other and promise quite interdisciplinary research directions ahead.

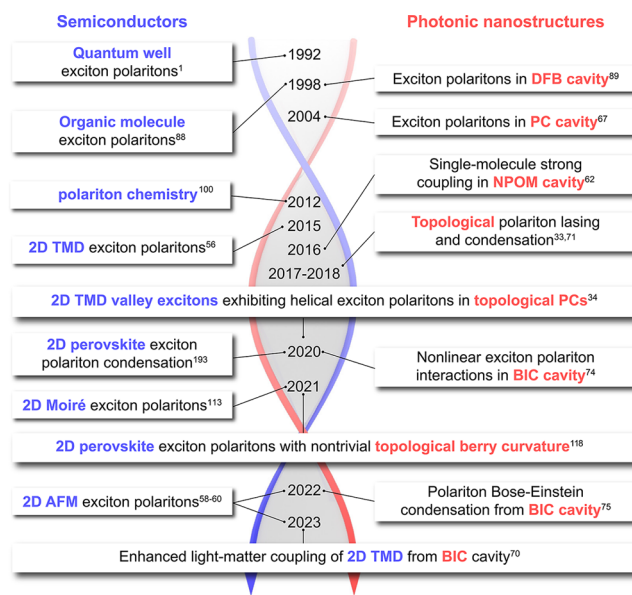


**Figure 2.** Timelines for the research progress of exciton polaritons with highlighted hallmarks.

Prior to 2015, exciton-polaritons had been observed sequentially in various semiconductors (e.g., quantum wells,<sup>1</sup> organic molecules,<sup>88</sup> bulk perovskites,<sup>89</sup> quantum dots,<sup>67,90</sup> etc.) integrated with conventional optical resonators (e.g., FP cavities, PC, etc.). Due to high crystalline quality and well controlled excitonic properties of quantum wells, exciton polaritons therein have demonstrated striking quantum phenomena and optoelectronic applications, such as Bose–Einstein condensation,<sup>2,16–18</sup> superfluidity,<sup>19–22</sup> quantum simulation,<sup>91–93</sup> and electrically pumped polariton lasers.<sup>94–96</sup> Because of large exciton binding energies of conventional semiconductors (e.g., organic molecules,<sup>88</sup> bulk perovskites,<sup>89</sup> ZnO,<sup>97,98</sup> GaN,<sup>99</sup> and Cu<sub>2</sub>O<sup>30</sup>), these quantum phenomena and optoelectronic applications have been gradually realized toward room temperature.<sup>3,5</sup> These hallmarks are mostly based on FP cavities and other photonic structures (e.g., distributed feedback cavities (DFB), grating structures, nanophotonic structures integrated with FP cavities, etc.). Among these photonic platforms, FP cavities are the most straightforward resonators, with well-studied photonic behaviors and mature fabrication techniques. Moreover, the FP cavities have been utilized to strongly couple with molecular vibrational states, so that the local chemical properties can be modified for an excellent frontier research topic, i.e., polariton chemistry.<sup>100–102</sup> For excitons of single photon emitters in the quantum dots,<sup>67,90</sup> FP cavities can hardly enable large enough coupling strength  $g$  for the strong coupling regime as the mode volume is not small enough. Therefore, pillar FP cavities and PC were exploited to increase the coupling strength by minimizing the mode volume, and ultimately the strong coupling regime was reached,<sup>67,90</sup> and even the quantum blockade effect was observed.<sup>25,31,32</sup>

After 2015, considerable attention has been shifted to emerging exciton-polariton systems that involve 2D semiconductors and distinct optical resonators with fascinating phenomena and control DOFs. 2D semiconductors mainly refer to TMDs and their heterostructures,<sup>38,45,46</sup> with recent inclusion of van der Waals 2DPK<sup>47,48</sup> and 2D AFM semiconductors.<sup>49,50</sup> Since the observation of 2D exciton

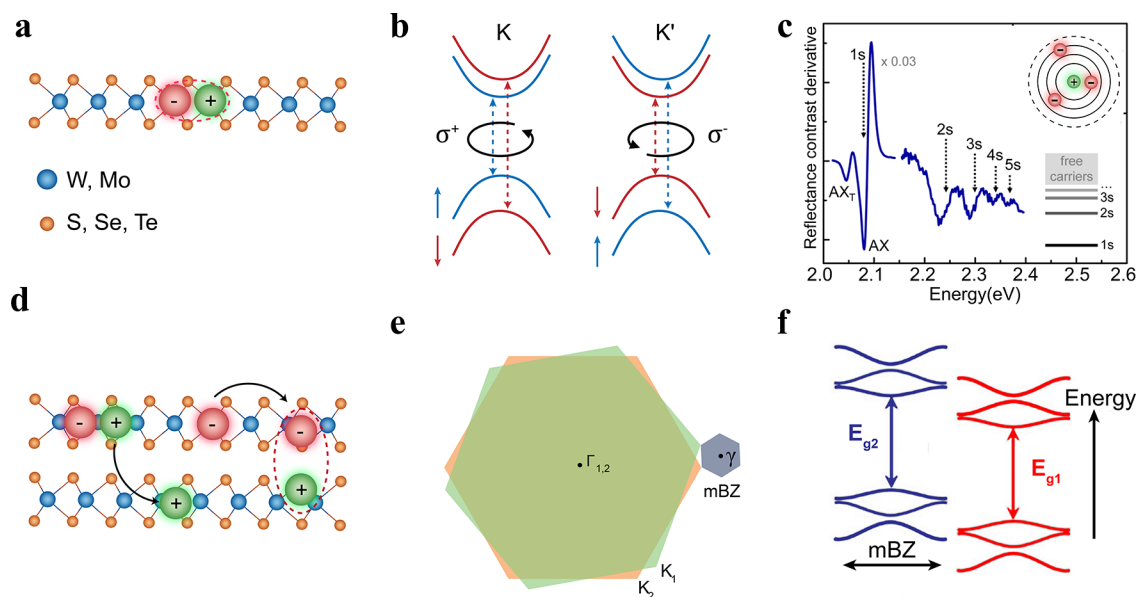


**Figure 3.** Schematics of excitons and their basic concepts in TMDs. (a) Schematic of intralayer exciton in a monolayer TMD, labeled by the red dashed box. (b) Diagrams of TMD valley energy bands. (c) Rydberg states of monolayer WS<sub>2</sub> exciton. (d) Schematic of excitons in TMD bilayer; the red dashed box represents interlayer exciton and black arrows show the charge transfer. (e) Moiré heterostructure Brillouin zone and (f) mini-Brillouin zone (mBZ) in a moiré heterostructure. Panel (a) reprinted with permission from ref 142. Copyright 2023 Springer Nature. Panel (c) reprinted with permission from ref 55. Copyright 2014 American Physical Society. Panel (d) reprinted with permission from ref 143. Copyright 2018 Springer Nature. Panel (e) reprinted with permission from ref 144. Copyright 2022 Springer Nature. Panel (f) reprinted with permission from ref 145. Copyright 2023 American Association for the Advancement of Science.

polaritons in TMDs at room temperature,<sup>56</sup> many inspiring discoveries have been reported. For example, valley polarization,<sup>103–105</sup> valley coherence,<sup>106,107</sup> valley Hall effect,<sup>108</sup> valley Stark effect,<sup>109</sup> and Zeeman effect<sup>110</sup> of TMD exciton polaritons have been extensively investigated. Recently, the nonlinear properties of such exciton polaritons have been also reported such as nonlinear bosonic interactions,<sup>111–113</sup> parametric scattering,<sup>114,115</sup> and polariton lasing.<sup>116,117</sup> Moreover, when the 2D excitons are hosted in 2DPK and 2D AFM semiconductors, exciton polaritons exhibit distinct control DOFs via the anisotropic nature of crystals<sup>57,118</sup> and strong magnetic responses.<sup>58,59</sup> Meanwhile, explorations of distinct optical resonators have been going beyond the traditional configurations of FP cavities and PC, extending to extreme nanophotonics of plasmonic nanocavities<sup>62,76–78</sup> and deliberately designed PCs with nontrivial topological photonic bands.<sup>10,15,33–35,70–75</sup> Along with the advancements of distinct photonic designs and nanofabrication techniques, these distinct optical resonators unveil fascinating photonic behaviors in the strong coupling regime, especially for 2D exciton polaritons. For example, optical resonators of plasmonic nanocavities can even realize the strong coupling at single molecule level at room temperature by leveraging advantages of nanometer-sized mode volume.<sup>62</sup> More interestingly, when PC are designed with nontrivial topological properties, exciton polaritons are found to demonstrate intriguing phenomena of quantum Hall effect<sup>33</sup> and quantum spin Hall effect,<sup>34</sup> prospecting tremendous opportunities to study correlated many-body physics and realize topological polaritonic device.

In the following sections of this Perspective, the fundamental excitonic properties of 2D TMDs would be first reviewed, and the strong coupling regime of 2D semiconductors with various optical resonators would be introduced and analyzed afterward. In these 2D exciton polaritons, attractive phenomena and the

underlying mechanisms are discussed in more details. Moreover, 2D exciton polaritons in emerging semiconductors of 2DPK and 2D AFM materials would be highlighted. Finally, our perspective with initial simulations on the exciton polaritons of these emerging semiconductors integrated with distinct optical resonators would be presented.

### Emerging Research of Exciton Polaritons in 2D TMDs.

**2D TMD Excitons.** TMDs are a class of materials with the formula MX<sub>2</sub>, where M is a transition metal element from group IV (e.g., Ti, Hf, Zr), group V (e.g., V, Nb, Ta), group VI (e.g., Mo, W), group VII (e.g., Tc, Re), or group X (e.g., Pd, Pt), and X is a chalcogen (S, Se or Te).<sup>119–121</sup> These materials form layered structures of X–M–X, where the chalcogen atoms are in two hexagonal planes separated by a plane of the metal atoms (similar to the schematic of Figure 3a). These layered materials include semimetals, superconductors, insulators, and semiconductors. In this Perspective, we will focus on discussing the most studied semiconducting TMDs for exciton polaritons, where the transition metal mainly refers to Mo or W and the chalcogen refers to S or Se. For the convenience, TMDs represent these semiconductors in this Perspective unless noted otherwise. TMD can be thinned down layer by layer because of weak interlayer interactions of van der Waals forces. When thinned down to monolayer limit, which only consists of two chalcogen atoms sandwiching a transition metal atom, TMDs become direct-bandgap semiconductors and possess strongly bound excitons of large oscillator strength and strong binding energies<sup>38,43,44</sup> (Figure 3a). Because of the 2D hexagonal lattice, the direct-gaps reside at two degenerate valleys at the hexagonal Brillouin zone of TMDs, denoted as K and K' (Figure 3b). The K and K' valleys are not equivalent and thus form valley excitons with time reversal symmetry, whose optical transitions follow distinct selection rule of circular polarizations.<sup>122–125</sup> Specif-

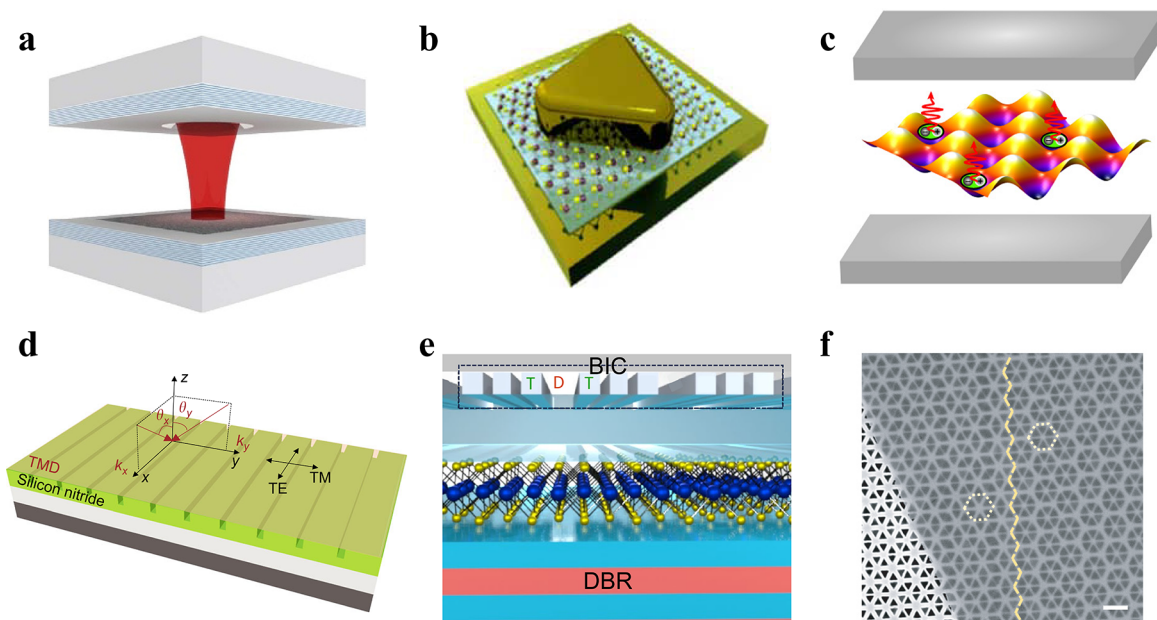


**Figure 4.** Schematics of various photonic systems of 2D TMD in the strong coupling regime. Schematics for (a) an open FP microcavity integrated with MoSe<sub>2</sub> and (b) an NPoM with monolayer WS<sub>2</sub>. (c) A FP cavity with moiré superlattices of MoSe<sub>2</sub>/WSe<sub>2</sub> heterostructures, (d) 1D PC with monolayer TMD, (e) BIC PC with monolayer WS<sub>2</sub>, and (f) topological PC with monolayer TMD. Panel (a) reprinted with permission under a Creative Commons Attribution 4.0 International License from ref 158. Copyright 2015 Springer Nature. (b) reprinted with permission from ref 172. Copyright 2020 American Physical Society. Panel (c) reprinted with permission from ref 113. Copyright 2021 Springer Nature. Panel (d) reprinted with permission under a Creative Commons Attribution 4.0 International License from ref 65. Copyright 2018 Springer Nature. Panel (e) reprinted with permission from ref 70. Copyright 2023 Springer Nature. Panel (f) reprinted with permission from ref 34. Copyright 2020 American Association for the Advancement of Science.

ically, each K (K') valley excitons can only allow optical transitions of left (right) circular polarization, providing photonic spin DOF for TMD excitons. Because of the large spin–orbit coupling of transition metals in TMDs, the split valence bands and conduction bands at each valley can also form different exciton species, including A and B excitons with quite distinct properties of absorptions and emissions (Figure 3b).<sup>122–125</sup>

In the research of the exciton polaritons in monolayer TMDs, A excitons of lower energy have attracted the most attentions because of the larger oscillator strength, strong binding energy and dominant emission properties.<sup>5,6,38,56</sup> In most cases, the excitons discussed in TMD monolayers refer to A excitons if no additional information is elaborated. For these specific properties, TMD excitons can also be understood by a hydrogen model with modifications of 2D confinement and dielectric screening.<sup>55</sup> Therefore, Rydberg series of 2D excitons can also be well resolved, even up to room temperature<sup>52,54,55</sup> (Figure 3c). It is worth noting that there could be dark excitons in W-based TMD monolayers, as the lowest energy transitions for A excitons are spin-forbidden and in turn form out-of-plane dipoles with respect to the 2D plane.<sup>126–130</sup> Moreover, due to the tightly bound nature and intrinsic excessive charge in monolayer TMDs, complex excitonic states including charged excitons (trions), biexcitons, and charged biexcitons<sup>131–136</sup> are also observed. These multiple-particle excitons generally have much weaker binding energies, which are comparable with the room temperature thermal energy ( $k_B T \sim 25$  meV), making them better resolved at low temperatures. Furthermore, they could also demonstrate valley polarization dependence for valley DOF, which depends on the electron–hole configuration for each specific case.<sup>131–136</sup>

Recently, another group of TMDs (ReS<sub>2</sub>, ReSe<sub>2</sub>) have also attracted some attentions, since they can also possess a direct band gap in the bulk form with large exciton binding energy and strong anisotropy.<sup>137,138</sup> The strong coupling regime in these TMDs of ReS<sub>2</sub>, ReSe<sub>2</sub> has been realized and may deserve further polaritonic investigations.<sup>139–141</sup>

Excitons in stacked TMD monolayers (homo/hetero-bilayers or moiré superlattices) have recently been found to demonstrate more intriguing optical properties with interlayer electronic coupling and moiré potential. In the stacked bilayer structures, along with the intralayer excitons, there emerges distinct interlayer exciton configuration<sup>143,146</sup> where electrons and holes are separated into different layers because of charge transfer and interlayer coupling (Figure 3d). These interlayer excitons, strongly depending on selected pairs of TMD monolayers, are typically referred to as either indirect-gap excitons or indirect excitons due to the type-II band alignments of the two monolayers.<sup>143,146</sup> This results in weak oscillator strength, which is generally smaller than the intralayer excitons by 2 orders of magnitude.<sup>147</sup> However, this oscillator strength could be significantly increased and would be beneficiary for the strong coupling regime if the interlayer excitons are hybridized with intralayer excitons.<sup>148–151</sup> The hybridization could occur when the interlayer excitons (IX) are close to the resonance of intralayer excitons, and the conduction (or valence) bands for both excitons are nearly degenerate. The hybridization of both excitons have been discovered in moiré superlattices of MoSe<sub>2</sub>/WS<sub>2</sub>, WS<sub>2</sub>/WSe<sub>2</sub>, bilayer MoS<sub>2</sub>, and bilayer MoSe<sub>2</sub>.<sup>148,149,151–153</sup> In these experiments, the IX were found to possess much larger oscillator strengths borrowed from the intralayer excitons and strong interactions with maintained dipolar interactions.

More striking phenomena and more intriguing underlying physics are expected when the moiré superlattices play a critical role for the exciton confinements.<sup>45,46,150,152,154–157</sup> The moiré superlattices could be much larger than the TMD atomic lattices when the twist angles of the stacked bilayers are small. Typically, at small twist angles, the moiré lattice constants are in the range of  $\sim 1$ – $10$  nm, constructing mini-Brillouin zone with mini-bands near the K ( $K'$ ) point (Figure 3e,f). These mini-bands act as localized potentials at moiré lattice sites that strongly modulate both the intralayer and interlayer excitons in TMD bilayers, enabling intriguing excitonic behaviors such as various optical selection rule, single-photon emission and strongly correlated quantum phenomena.<sup>45,46,150,152,154–157</sup> When coupling these moiré superlattices with optical resonators, attractive many-body interactions with moiré confinements and tunable arrays of quantum emitters based on strong correlation models (e.g., Bose–Hubbard model) are expected.<sup>145</sup> In a recent experimental report of moiré exciton polaritons, the quantum dot-like nonlinearity in moiré superlattices is observed, suggesting many possibilities of polariton blockade and strongly correlated polariton gases with electrical tuning.<sup>113</sup>

Furthermore, it is worth noting that 2D platform is ideal to integrate different materials together to study intriguing physics, including not only stacked TMDs such as moiré superlattices but others like magnetic semiconductors, dielectric layer, or other types of 2D materials.

**Investigation of the Strong Coupling Regime in 2D TMDs.** For these distinctive excitonic properties, TMDs as the most promising and feasible 2D semiconductors have been investigated to explore beyond the limitations of conventional semiconductors in the strong coupling regime. Since 2015, the strong coupling of TMD excitons has been realized in various photonic systems, where distinct control DOFs and attractive phenomena have been discovered.<sup>5,6,56,113,158</sup>

The straightforward way to reach the strong coupling regime of monolayer TMD excitons is based on general FP cavities.<sup>56,158,159</sup> For example, in the conventional FP cavity (Figure 1d) structure, the strong coupling of monolayer MoS<sub>2</sub> was realized at room temperature with a Rabi splitting of  $\sim 46$  meV.<sup>56</sup> This cavity configuration was later optimized to demonstrate robust strong coupling with reasonably high splitting-to-line width ratio (SLR) of  $\sim 3.3$ , which can support coherent control of polariton emission and dynamics from low temperature through room temperature.<sup>86</sup> Sequentially, the FP cavity was modified to an open cavity with a nanotranslated top mirror of DBR (Figure 4a), and the strong coupling of monolayer/bilayer MoSe<sub>2</sub> was also realized with high SLR at low temperatures.<sup>158</sup> Since FP cavities were found to be such a convenient platform for the strong coupling of TMD excitons, a simpler configuration of DBR-metal film could also work.<sup>159</sup> Recently, FP cavities of two metal films controlled by Casimir forces were also demonstrated to be capable of supporting the strong coupling regime at room temperature.<sup>160</sup> In a similar metal film FP cavity integrated with electrodes, the coupling strength of polaritons could be reduced as the applied voltage increases, due to reduced oscillator strength of excitons in WS<sub>2</sub> by the screening of Coulomb interaction with increased free carriers.<sup>161</sup> Moreover, the strong coupling regime has also been observed for charged excitons (trions) and higher Rydberg states of excitons in TMD monolayers within FP cavities.<sup>112,162–167</sup> Different dispersion features and nonlinear interactions were discovered in the strongly coupled polaritons

of the distinct exciton species. Note here that most of the strong coupling regimes discussed above were confirmed via the criteria based on eq 5.

By leveraging the advantages of the atomic thickness, the plasmonic nanocavities were also tried out to determine if the small mode volume could facilitate a strong coupling regime. To minimize the influences of plasmonic lossy feature (broad line width), plasmonic arrays with narrower mode line widths have been tested to realize the strong coupling.<sup>81,82</sup> However, the mode volume of these plasmonic arrays remained comparable to the wavelength volume. Plasmonic nanocavities of NPoM and bowties were tried for few-layer TMDs,<sup>167,168</sup> and NPoM was later tested for monolayer TMDs<sup>169–171</sup> to realize the strong coupling regime, where the criteria of eq 5 were not fully satisfied in some examples. Subsequently, the strong coupling regime of monolayer TMDs was confirmed in NPoM configurations (Figure 4b) of nanoprism and core–shell nanospheres.<sup>172,173</sup> In these NPoMs, the criteria of eq 5 were fully satisfied, and the small mode volume (generally below  $50 \text{ nm}^3$ <sup>362,167</sup>) was exploited to look into the coupling behaviors of few excitons and nonlinear optical behaviors. However, the lossy nature (broad line widths) of these plasmonic nanocavities still hinders further investigation of the exciton polaritons' PL, although the FP modes of plasmonic nanorod could help improve their PL characteristics.<sup>174</sup>

In these conventional optical resonators, the strong coupling of 2D excitons in TMD bilayers has also been realized. Because of the much smaller oscillator strengths ( $f$ ),<sup>147</sup> interlayer excitons need to hybridize with intralayer excitons for larger oscillator strength<sup>148–151</sup> and thus larger coupling strength ( $g \propto \sqrt{f/V}$ , where  $V$  is the mode volume) with optical resonators. The interlayer excitons in bilayer MoS<sub>2</sub> can be efficiently hybridized with intralayer A excitons, and therefore could be demonstrated to reach the strong coupling regime in a FP cavity and enhance polaritonic nonlinear interactions.<sup>175</sup> These hybridized excitons could be efficiently modulated through moiré superlattices, leading to the observation of moiré exciton polaritons with enhanced nonlinear interactions (Figure 4c).<sup>113</sup> The enhanced nonlinear interactions in the bilayer MoS<sub>2</sub> demonstration were attributed to the dipolar interactions of these hybridized excitons,<sup>175</sup> while those in the moiré exciton polaritons were due to the moiré potential confinements.<sup>175</sup> Moreover, they could be easily tuned by electrical doping for strongly correlated physics.<sup>45,46,176</sup> As a result, these hybridized exciton polaritons were predicted with more profound quantum phenomena of many-body physics and more extensive polaritonic applications.<sup>145</sup>

In comparisons with FP cavities and plasmonic nanocavities, PC can easily support much higher quality factor but possess appropriate mode volume for the strong coupling regime.<sup>61,64</sup> The strong coupling in 1D PC was achieved with monolayer WSe<sub>2</sub> and WS<sub>2</sub> for anisotropic polariton dispersions of the TE and TM modes (Figure 4d). Besides, the PC can support extremely high quality factor for different configurations. One is based on specific surface mode, referred to Bloch surface wave (BSW) in DBR, can realize the strong coupling of monolayer WS<sub>2</sub>.<sup>111</sup> Another one is based on BIC, whose quality factor ideally could get to infinity, can also easily support the strong coupling regime of TMD monolayers<sup>70,74,177</sup> (Figure 4e). In these cases of high quality factors, the nonlinear interactions among 2D exciton polaritons

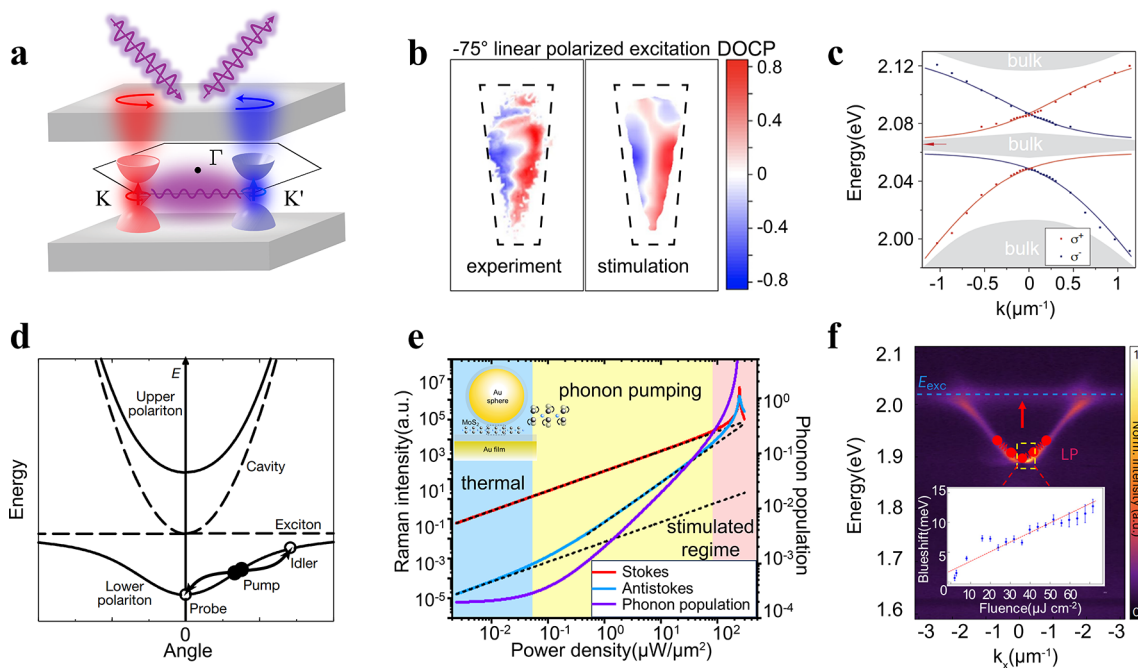


**Figure 5.** Fascinating phenomena of exciton-polaritons in 2D TMDs. (a) Schematic of valley polarization and valley coherence in 2D exciton polaritons. (b) Valley Hall effect of exciton-polaritons in monolayer MoSe<sub>2</sub> under linear polarization excitation. Left panel: experimental data; right panel: simulated data. Dashed box represents the sample region. (c) Helical polariton propagation in edge state within 2D topological PC of photonic spin Hall effect. (d) Configuration schematic for the parametric scattering of exciton polaritons. (e) Nonlinear phonon scattering under strong coupling regime in plasmonic nanocavities of NPoM. The nonlinear phonon regime resides after the linear thermal regime and nonlinear anti-Stokes (phonon pumping) regime. (f) Nonlinear interaction of exciton polaritons in BIC, inset is the blue shift of LP with increasing pump fluence. Panel (b) reprinted with permission from ref 108. Copyright 2019 Springer Nature. Panel (c) reprinted with permission from ref 34. Copyright 2020 American Association for the Advancement of Science. Panel (d) reprinted with permission from ref 178. Copyright 2001 Springer Nature. Panel (e) reprinted with permission from ref 173. Copyright 2021 Springer Nature. Panel (f) reprinted with permission from ref 70. Copyright 2023 Springer Nature.

are all found to be enhanced significantly. Meanwhile, 2D topological PCs were also explored to realize the strong coupling of 2D excitons (Figure 4f), by leveraging advantages of the valley DOF and 2D excitonic nature.<sup>34,35</sup> These topological PCs not only can be easily integrated with 2D TMDs via nanofabrication techniques but also can support high quality factor and modulate the mode volume with topological protection for the strong coupling regime. In this context, these 2D topological exciton polaritons were then demonstrated for the quantum spin Hall effect as well, prospecting many exciting opportunity to study the many-body physics and develop polaritonic devices.<sup>10,15,33–35,70–75</sup>

**Fascinating Phenomena in 2D Exciton Polaritons.** For the hybrid nature leveraging the advantages of exciton and photon constituents, 2D exciton polaritons in these photonic systems discussed above exhibit attractive phenomena. In the following, these phenomena would be surveyed based on the underlying mechanisms, such as distinct valley DOF, bosonic nonlinear interactions, and their potential with topological structures.

**Valley Exciton Polaritons.** 2D exciton polaritons can directly inherit the valley DOF from TMD excitons and thus demonstrate this diverse control DOF and anticipated dynamics that conventional exciton polaritons cannot provide. For the valley DOF, as mentioned above, the straightforward feature is the optical transition rule of circular polarization dependence.<sup>122–125</sup> Valley polarization dependence was demonstrated by three groups in 2017,<sup>103–105</sup> so that the valley DOF is better preserved in 2D exciton polaritons than

bare valley excitons and can persist up to room temperature (Figure 5a). In some cases of electrical doping conditions, valley DOF was even observed in trion polaritons.<sup>105,106,110</sup> The preservation of valley DOF in these demonstrations is attributed to the coherent coupling process that hinders the depolarization dynamics of valley excitons. Equipped with valley DOF, optical manipulations of 2D exciton polaritons were further demonstrated at external fields such as an ultrafast light pulse and magnetic field. In an optical configuration of pump–probe, valley-selective Stark effect was observed in a FP cavity with monolayer WS<sub>2</sub>, where the Stark shifts can only be observed when the light of pump and probe is cocircularly polarized.<sup>109</sup> By applying a magnetic field, Zeeman splitting between valley excitons polaritons could be observed;<sup>179,180</sup> this splitting could be largely enhanced by proximity effect if the monolayer TMD is placed on top of magnetic substrate (EuS) in a cavity.<sup>110</sup>

This distinct valley DOF brings up intriguing topics for further fundamental study and photonic applications of 2D exciton polaritons, such as valley coherent dynamics and the valley Hall effect. The valley coherent dynamics was observed in the linear polarization dependence of bare valley excitons.<sup>125,181</sup> For TMD valley excitons, the linear polarization angle could represent the dynamic correlated phase between K and K' valleys when linear polarization is decomposed as the superposition of two crossed-circular polarizations. The linear polarization angle of valley exciton PL is found to follow the polarization angle of pump light, suggesting the coherent valley dynamics in TMD exci-

tons.<sup>125,181</sup> The valley coherence time is quite short and estimated to be a few picoseconds and thus can hardly be captured at room temperature because of more complex dynamics from the thermal process. The valley coherence was ultimately observed in 2D exciton polaritons of WSe<sub>2</sub> even up to room temperature<sup>106,182</sup> (Figure 5a). This is because the strong coupling process provides a coherent dynamic channel that protects the valley coherence from dephasing processes at an elevated temperature. Valley Hall effect refers to that the carriers/excitons from different valleys would be drifted in opposite directions perpendicular to the transport pathways, which was predicted earlier in graphene,<sup>183</sup> and ultimately observed in a transistor of monolayer MoS<sub>2</sub>.<sup>184</sup> The valley Hall effect is regarded as a critical mechanism for valleytronic applications,<sup>185</sup> and was also observed in MoS<sub>2</sub> excitons.<sup>186</sup> This effect was reported recently in 2D exciton polaritons, where high valley coherence was preserved via the second harmonic generation (SHG)<sup>108</sup> (Figure 5b). Another efficient way to observe similar valley transport phenomena is to couple the TMD excitons with topological PC for quantum spin Hall effect<sup>34,35</sup> (Figure 5c). Following the nontrivial bands, different valley exciton polaritons in the strong coupling regime of such topological PC would propagate in the opposite directions with crossed-circular polarizations.<sup>34,35</sup> The topological nature of such 2D exciton polaritons will also be discussed in more detail in a later context.

**Bosonic Nonlinear Interactions.** Bosonic nonlinear interactions are the fundamental driving mechanism for the quantum phenomena and photonic applications in exciton polaritons, such as BEC, superfluidity, and quantum simulation.<sup>2,22,187</sup> As there is negligible interaction between photons, the nonlinear interactions of exciton polaritons can only be originated from the exciton constituent, which is thus proportional to their excitonic fractions (the exciton Hopfield coefficients, “X”) and is ultimately limited by the exciton interactions. The exciton interactions in 2D TMDs mainly include two aspects, i.e., exchange interactions and dipole–dipole interactions.<sup>2,22,187</sup> The former one scales as  $E_B a_B^2$  (where  $E_B$  and  $a_B$  are the exciton binding energy and Bohr radius respectively), the latter one strongly depends on the transition dipoles of these excitons (the dipole length, the dipole alignments, etc.). For most of discussed cases in this Perspective, these bosonic interactions behave as repulsions and are usually observed as spectral blueshift ( $\Delta E_{\text{ex}}$ ) with increased exciton density ( $n_{\text{ex}}$ ), which is quantified by the interaction strength ( $g_{\text{ex}}$ ) as  $\Delta E_{\text{ex}} = g_{\text{ex}} n_{\text{ex}}$ . Note here that  $g_{\text{ex}}$  may include contributions from exchange interactions and dipolar interactions depending on the exciton configurations.

In the strong coupling regime, polariton interactions are also characterized by the spectral shift ( $\Delta E_{\text{pol}} = g_{\text{pol}} n_{\text{pol}}$ ), where  $g_{\text{pol}}$  refers to the polariton–polariton interaction strength and  $n_{\text{pol}}$  is the polariton density. The polariton interaction strength  $g_{\text{pol}}$  could be understood by two main contributions, i.e., excitonic interactions with  $g_{\text{pol-ex}}$  and phase space filling (PSF, also known as saturation effect) with  $g_{\text{pol-sat}}$ .<sup>2,22,187</sup> The contribution of  $g_{\text{pol-ex}}$  is originated from the excitonic constituent and scales as  $X^2 g_{\text{ex}}$ , where  $X$  is the excitonic Hopfield coefficient.<sup>2,22,187</sup> The contribution of  $g_{\text{pol-sat}}$  is resulted from the weakened coupling strength by the PSF when the polariton density approaches saturation.<sup>2,22,187</sup> Typical feature for PSF with decreasing coupling strength is that the lower polariton states blueshift while the higher polariton states redshift and

$g_{\text{pol-sat}} \propto X^2 \Omega_R$ . Practical understanding of these nonlinear interactions needs careful analysis of all these contributions.

With the nonlinear interactions, exciton polaritons may form BEC with the following process: at low polariton densities, exciton polaritons would follow Bose–Einstein distribution with thermal equilibrium; at high densities, the nonlinear interactions between polaritons may induce stimulated bosonic scattering and redistribute the exciton polaritons into the energy favorable states (generally the lowest polariton states); the majority occupation of these polaritons at the favorable states could lead to spontaneous coherent bosonic condensate, which is regarded as BEC.<sup>2,5,6,22,187</sup> In practical experiments, the spontaneous coherence of the polariton condensate could be observed as a research focus, although the BEC may not be strictly realized because thermal equilibrium cannot be always reached and phonon scattering may interfere the stimulated bosonic scattering.<sup>2,5,6,22,187</sup> The nonlinear interactions have been one of the most important research topics since the realization of 2D exciton polaritons. The earliest study of nonlinear interactions was conducted in BSW-polaritons based on a DBR-WS<sub>2</sub> configuration.<sup>111</sup> The nonlinear interactions in terms of spectral blue-shift were found to support extremely long polariton propagations of up to 33.4  $\mu\text{m}$ . They were characterized by polariton interaction strength  $g_{\text{pol}} \sim 6 \times 10^{-4} \mu\text{eV} \cdot \mu\text{m}^2$  and pure exciton strength as  $g_{\text{ex}} \sim 6 \times 10^{-2} \mu\text{eV} \cdot \mu\text{m}^2$ . The interaction strength was found to be smaller than the theoretical predictions by more than 1 order of magnitude, which was attributed to overestimated polariton density and unknown complex excitonic mechanisms. The nonlinear interactions were further studied in FP cavities of 2D TMDs, and the strength  $g_{\text{ex}}$  was mostly reported at the range of  $10^{-1} \sim 10^{-2} \mu\text{eV} \cdot \mu\text{m}^2$  (see Table S1 in Supporting Information of ref 114). These observations suggest that the nonlinear interactions in 2D exciton polaritons may not be that strong for the bosonic stimulation at finite polariton densities, which are critical for the quantum phenomena such as BEC. To examine the bosonic stimulation, an effective configuration is based on parametric scattering scheme (the so-called “magic angle” excitation scheme) as in Figure 5d.<sup>178,188</sup> Here the polaritons are resonantly injected by a pump laser at the magic angle. The magic angle (corresponding to one specific in-plane wavenumber,  $k_p$ ) is chosen to allow energy and momentum conservation for the scattering between two polaritons. In this way, one polariton is scattered into the lowest-energy state ( $E_{k=0}$ ) and the other into a higher-energy state ( $E_{2k_p}$ ) to fulfill the eq  $2E_{k_p} = E_{2k_p} + E_{k=0}$ , where  $E_{k_p}$  is the pump laser energy. A weak probe beam (the “signal” with  $E_{k=0}$ ) is applied at normal incidence to stimulate the scattering into the lowest-energy state with a superlinear increase (amplification) of polaritons at  $E_{k=0}$ , which could be regarded as optical parametric amplification (OPA). The parametric scattering is therefore modeled by coherent bosonic final-state stimulation with nonlinear polariton-polariton interactions. This parametric scattering was recently reported with interaction strength ( $\sim 10^{-1} - 10^{-2} \mu\text{eV} \cdot \mu\text{m}^2$ ) and improved valley DOF in the nonlinear regime.<sup>114,115</sup> Moreover, the BEC-like polariton condensation has also been reported recently,<sup>116,117</sup> indicating profound opportunities to investigate the quantum phenomena in 2D exciton polaritons. One of differences between the resonant pumping scheme of parametric scattering and nonresonant pumping scheme of BEC is minimizing the phonon scattering. Phonon scattering becomes a critical

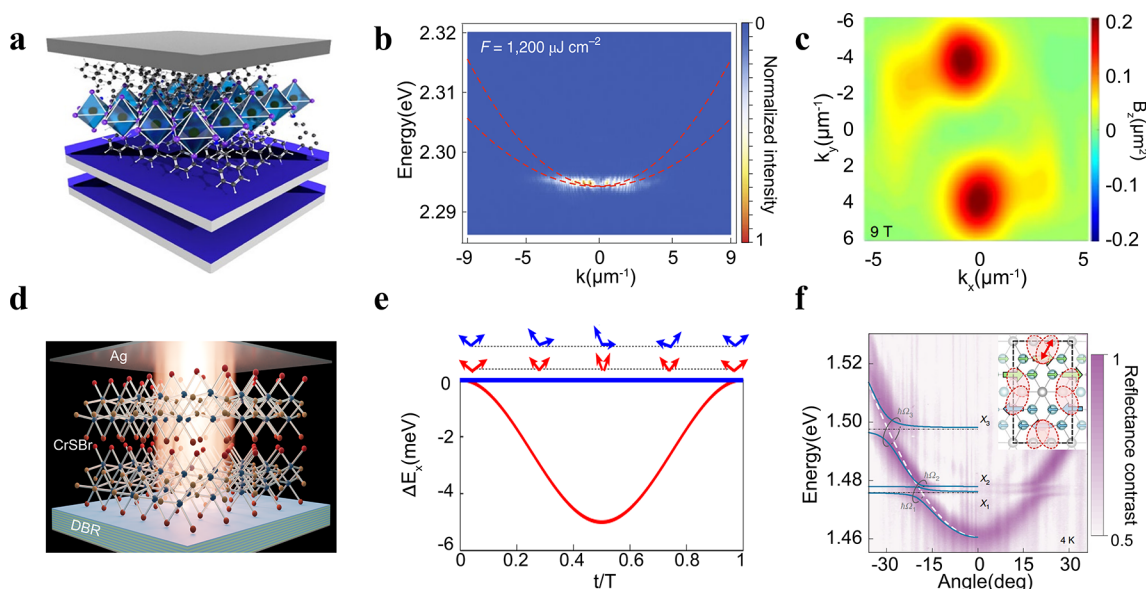


**Figure 6.** Strong coupling in 2DPK and 2D AFM Materials. (a) Schematic of a FP cavity integrated with 2DPK ( $\text{F}(\text{C}_6\text{H}_5(\text{CH}_2)_2\text{NH}_3)_2\text{PbI}_4$ ). (b) Room-temperature exciton-polariton condensation in 2D perovskite. (c) Nonzero Berry curvature through control of an external magnetic field in 2D perovskite. (d) Schematic of CrSBr integrated with a FP cavity. (e) Coherently hybridized excitons with magnons in CrSBr. (f) Energy dispersion of polaritons; inset is Zhang–Rice excitons in NiPS<sub>3</sub>. Panels (a) and (c) reprinted with permission from ref 118. Copyright 2021 Springer Nature. Panel (b) reprinted with permission from ref 193. Copyright 2020 Wiley Publishing Group. Panel (d) reprinted with permission under a Creative Commons Attribution 4.0 International License from ref 60. Copyright 2023 Springer Nature. Panel (e) reprinted with permission from ref 198. Copyright 2023 Springer Nature. Panel (f) reprinted with permission from ref 58. Copyright 2022 Springer Nature.

process for exciton polaritons at elevated temperatures and directly acts on the valley dynamics for 2D exciton polaritons up to room temperature. Nonlinear valley phonon scattering was recently observed in plasmonic nanocavities, where the phonon scattering was enhanced drastically by the 2D exciton polaritons with valley polarization dependence and could support the stimulated scattering under resonant pump condition (Figure 5e).<sup>173</sup>

The enhancement of nonlinear interactions has been tried out in various approaches, which have been one of the research focuses in 2D exciton polaritons. One of the straightforward ways is to utilize multiple quantum well structures with higher exciton polariton density.<sup>158</sup> This configuration, on the one hand, indeed enhances the coupling strength of 2D exciton polaritons and could even enable the polariton light-emitting devices.<sup>189</sup> More importantly, on the other hand, it significantly increase the saturation density of exciton polaritons for the nonlinear processes, which is indeed observed with strong PSF.<sup>190</sup> Though the nonlinear interactions are enhanced, the interaction strength is still comparable to the single monolayer case. To enhance the interaction strength, an effective way is leveraging advantages of larger Bohr radius of Rydberg excited states of excitons by following  $E_B a_B^2$ .<sup>191</sup> When strongly coupled with FP cavity, polaritons of Rydberg excitonic state (2s) demonstrate an enhancement of 4.6 for the nonlinear interactions than those of ground exciton states.<sup>112</sup> Another way of enhancing the interactions is to exploit the dipole–dipole interactions from dipolar alignments of the bilayer TMDs. As discussed above, the interlayer excitons possess an out-of-plane dipole component that significantly increases excitonic interactions. When hybridized with intralayer excitons, they can also strongly couple with FP cavities for enhanced nonlinear interactions, which were indeed observed with an enhancement of 10 in a polaritonic

system of bilayer MoS<sub>2</sub>.<sup>175</sup> More interestingly, when the bilayer excitons are trapped in moiré superlattices, the nonlinear interactions could be even enhanced with moiré potential trap (Figure 4c).<sup>113</sup>

Besides manipulating the exciton constituent for stronger interactions, distinct photonic structures (e.g., topological photonic structures) could also play a nontrivial role in enhancing the nonlinear polariton interactions, which are though less explored so far. Typical examples have been tried out are based on the photonic structures of BIC.<sup>70,74</sup> As discussed above, BICs are typically featured by their high quality factor, which could dramatically decrease the photonic loss.<sup>64</sup> Due to the high quality factor, the 2D exciton polaritons in BICs were discovered with stronger coupling strength and similar nonlinear interactions to other polaritonic systems, but with topological protection from defects or fabrication imperfections.<sup>70,74</sup> Though not extensively investigated yet, topological photonic structures, as we emphasize here, would be an efficient way to enhance the nonlinear polariton interactions for following arguments.<sup>11,12</sup> First, the high quality factor is beneficial to minimize the photonic loss of exciton polaritons, which could be obtained in various topological structures. As exemplified above, photonic structures of BIC (other than the demonstrated ones<sup>70,74</sup>), photonic valley Hall, and higher order corner states could also support high quality factors. Second, the mode volume could be significantly minimized by some topological PCs of photonic valley Hall and higher order corner states. The optimum resonators for exciton polaritons and their nonlinear interactions require a large quality factor and small mode volume, which could be satisfied in topological structures. For example, while maintaining high quality factors, the photonic structures of corner states could support a smaller mode volume than PC defect cavities. Last but not least, the topological structures

could have topological protections from defects. The defects, from either 2D TMDs or photonic structures, could result in scattering loss and even involve phonon scattering, which are detrimental to the nonlinear interactions. The topological protections in 2D exciton polaritons, if realized, are expected to be critically beneficial for the quantum phenomena and nonlinear optics. For this aspect, we elaborate how these arguments are substantiated in some specific cases with numerical simulations in the following “Outlook” section.

**Emerging 2D Semiconductors for Exciton Polaritonic Research.** Along with the progress in 2D TMDs, emerging 2D semiconductors were discovered as fascinating platforms to study intriguing polaritonic phenomena with strong anisotropy and magnetic control. Specifically, two groups of 2D semiconductors for polaritonic research are surveyed as following.

**2D Perovskites (2DPK).** With large oscillator strength and strong binding energy, excitons of 2DPK were found to support higher PL quantum yield, higher nonlinear interaction strength and strong anisotropy for polariton research, in comparisons with 2D TMDs.<sup>47,48,57</sup> Here 2DPK mainly refers to Ruddlesden–Popper halide perovskites (RPP) of quantum well structures formed by 2D layers of halide perovskites separated by bulky organic spacer layers. Their stoichiometric ratios are defined by the general formula  $A_2A'_{n-1}M_nX_{3n+1}$  where A, A' are cations, M is a metal, X is a halide and the integer value  $n$  determines the perovskite layer thickness (i.e., the quantum well thickness with values of  $n$  up to 5).<sup>47,48</sup> Each layer of 2DPK (for smaller  $n$  values) has similar 2D quantum confinement and dielectric screening environment to the 2D TMDs, leading to large oscillator strength and strong binding energies (even up to 470 meV) for 2DPK excitons, as compared to conventional 2D semiconductors characterized by Wannier–Mott excitons. As  $n$  increases and is larger than 5, 2DPK becomes similar to 3D perovskites without prominent 2D nature.<sup>47,48</sup> The interlayer interactions between 2DPK layers are much smaller than 2D TMDs, and thus can construct multiquantum well structures without interferences from neighbored quantum well. Together with direct-gap structures of high transition probabilities, 2DPK excitons demonstrate a high PL quantum yield and support higher density for stronger nonlinear interactions. Moreover, 2DPK are found to be stable at some specific anisotropic structural phase and easy to alter the organic/inorganic component that renders strong optical anisotropy and rich tunability for photonic applications.<sup>47,48</sup> Here we mainly survey the research progress of exciton polaritons in the strong coupling of 2DPK.

Similar to 2D TMDs, 2DPK can also easily reach the strong coupling regime, which were realized in FP cavities at room temperature<sup>57,192</sup> (Figure 6a). With strong nonlinear interaction and higher polariton density, the polariton condensation was also demonstrated in 2DPK exfoliated from single crystals<sup>193</sup> (Figure 6b). Interestingly, due to the strong anisotropy, 2DPK can be also exploited to investigate the nontrivial topological nature of the polariton bands by two examples. Here, the anisotropy would be divided into optical anisotropy of the cavity and structural anisotropy of 2DPK for clarity. The first one combines 2D perovskites with liquid crystals in a FP cavity for a huge Rashba–Dresselhaus spin–orbit coupling (SOC) via the splitting of TE and TM modes to support optical anisotropy.<sup>194</sup> In this way, the Berry curvature of the polariton bands can be quantitatively controlled by electrically tuning the orientations of the liquid crystal. The

local Berry curvature is found to be nonzero, but the integral Berry curvature remains zero since the time-reversal symmetry is not broken, which is similar to those discovered in anisotropic 3D perovskites<sup>195,196</sup> and anisotropic organic molecule.<sup>197</sup> The other example introduces a Zeeman effect via an external magnetic field in an anisotropic polariton system of FP cavity, which leverages full advantages of the anisotropic 2DPK.<sup>118</sup> With strong Rashba–Dresselhaus SOC, nonzero Berry curvatures were measured (Figure 6c). Different from the first example, a nontrivial topological gap is opened between the split modes and the integral Berry curvature is nonzero because the time-reversal symmetry is broken. These attempts indicate a distinct way to control the topological properties in the polariton bands without relying on specific topological PC structures.

**2D Antiferromagnetic (AFM) Semiconductors.** Since the discovery of 2D magnetism in 2017,<sup>199,200</sup> 2D magnetic semiconductors have attracted extensive attentions for fascinating magneto-optical phenomena.<sup>201</sup> Recently, 2D excitons in AFM semiconductors, such as CrSBr and NiPS<sub>3</sub>, have been discovered with attractive magnetocorrelated features that are intriguing for exciton polariton research. Among these features, excitons coupled with magnons provide a distinct degree of freedom to impact the strong coupling regime, manipulate the spin nature of the polaritonic quantum system, and prospect distinct spintronic information processing with exciton polaritons. Magnons, defined as quantization of spin waves in the collective oscillations of electron spins, can be found to be strongly coupled with an archetypal AFM semiconductor of CrSBr. It consists of ferromagnetic (FM) monolayer films with interlayer AFM coupling along the stacking direction, which can be transformed into FM order under an external magnetic field.<sup>50</sup> The AFM and FM orders provide quite distinct band structures, leading to spin-correlated excitons in CrSBr with strong anisotropy, exhibiting giant oscillator strength (much larger than 2D TMDs), high PL quantum yield, and extremely strong anisotropy. Moreover, they can efficiently couple with the magnons that can be directly observed in ultrafast time-resolved spectroscopy,<sup>202</sup> presenting an outstanding candidate for the strong coupling regime with magnetic control.

Another example of NiPS<sub>3</sub>, featuring nickel spin chains with ferromagnetic alignment, exhibits AFM arrangement at each layer below the Neel temperature  $T_N \sim 155$  K. In the AFM order, there emerge spin–orbit entangled excitons originated from the many-body state of Zhang–Rice singlets, which are fundamentally different from the conventional Wannier–Mott excitons formed by extended Bloch states.<sup>49</sup> These excitons coexist with the AFM order, and are featured with large oscillator strength, extremely sharp PL line width (typically <1 meV) and strong optical anisotropy,<sup>49,203,204</sup> which could be fully exploited in the strong coupling regime.

The research of the strong coupling regime of AFM semiconductors is still at its initial stage, which would be surveyed with the typical examples of CrSBr and NiPS<sub>3</sub>. In a DBR FP cavity of CrSBr, the excitons are found to reach the ultrastrong coupling regime with extremely large coupling strength (Figure 6d).<sup>59,60</sup> Furthermore, because of the high index, extremely large oscillator strength, and the optical paths of a few hundreds of nanometers, CrSBr can form an internal FP cavity by itself, which supports cavity mode and can even reach the strong coupling regime without external optical cavity. In addition, these exciton polaritons have demonstrated

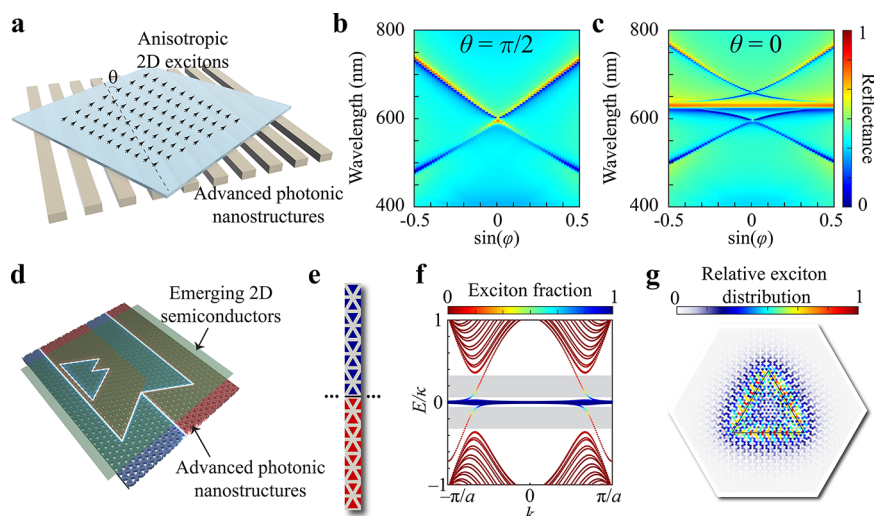


**Figure 7.** Outlook on 2D exciton polaritons integrated with photonic nanostructures. (a) Illustration of anisotropic 2D excitonic materials integrated with photonic nanostructures exhibiting topological charges in momentum space. The relative angle  $\theta$  between the exciton dipoles and the photonic structures can be used to control strength of light-matter interactions from the weak coupling to the strong coupling regimes. (b, c) Calculated angular-resolved reflectance spectra for  $\theta = \pi/2$  and 0 respectively. (d) Schematic illustration of topological nanophotonic crystals integrated with emerging 2D exciton systems. (e) Structure of topological boundaries between two regions of PCs with opposite topological order, which support topological edge states at the domain wall. (f) Calculated band diagrams of exciton-polariton topological edge states. Valley-polarized half-exciton half-light topological edge states exist in the bulk band gaps (marked with a gray shadow). (g) Calculated spatial distribution of relative exciton distributions for the eigenstates inside the topological bulk bandgap.

strong anisotropic features following their exciton fraction. As the energy of excitons varies from AFM to FM orders, the exciton polaritons can be largely detuned by applying appropriate external magnetic fields, leading to controllable contributions from excitons and photons.<sup>59,60</sup> Specifically, the interaction between excitons and magnons influences the exciton resonances' shifts as a function of magnetic moment angle between adjacent layers, leading to cosine-function-like shifts in exciton resonances and polariton states (Figure 6e).<sup>60</sup> Moreover, magnons, quantum excitations of spin waves, can also efficiently couple with exciton polaritons in CrSBr inherited from their exciton constituent under external magnetic field.<sup>59</sup> For the AFM semiconductor of NiPS<sub>3</sub>, the strong coupling between photons and spin-correlated excitons in a FP cavity generates distinct exciton polaritons that inherit characteristics of excitons, photons, and spins (Figure 6f).<sup>58</sup> Because the spin-correlated excitons cannot efficiently couple with phonons at low temperatures, most phonons cannot facilitate relaxation of polarized excitons to the lower polaritons and lead to polariton bottleneck relaxation and dominant PL emissions around the uncoupled exciton resonance. As temperature increases, the phonon scattering is enhanced so that the polariton bottleneck relaxation is reduced, and stronger emission can be observed at lower polariton states. By analyzing the excitation density, exciton resonances, and their relations with Rabi splitting, the exciton polaritons in NiPS<sub>3</sub> are found to be quite localized without strong long-range nonlinear interactions.<sup>58</sup> This is attributed to the tightly bound localized excitons in NiPS<sub>3</sub> and their influence on polariton research, which may merit further investigations. Though at its initial stage, the polariton study of 2D AFM semiconductors provides distinct DOF of magnetic control, promising unconventional magneto-optics for the polaritonic phenomena.

**Outlook on the 2D Exciton Polaritons and Their Nonlinear Interactions.** From the above review, the rapid research progress of the strong light-matter coupling benefits from the developments of two interwinding directions, i.e., innovative 2D semiconductors and fascinating photonic nanostructures, as in Figure 2. By further leveraging full advantages of the latest progresses from these interwinding directions, there is still plenty of room to explore fascinating polaritonic quantum phenomena. Here our outlook on the 2D exciton polaritons would be presented from semiconductor perspective and photonics perspective as the following, where numerical simulations for some specific cases are carried out to claim the possibility.

From the semiconductor perspective, integrating various cutting-edge 2D exciton systems, such as moiré superlattices, 2DPK, and 2D AFM semiconductors with photonic nanostructures, could potentially create distinct ways to manipulate strong light-matter coupling at the nanoscale with distinct DOF. For example, 2DPK and 2D AFM display excitons with highly anisotropic dipoles, as discussed above and indicated in Figure 7a. By combining these 2D materials with anisotropic photonic nanostructures, we can continuously regulate the strength of light-matter coupling by adjusting the relative angles  $\theta$  between the exciton dipoles and the nanostructures. Specifically, we are considering a 1D BIC grating that supports nontrivial topological charges in momentum space (Figure 7a). By controlling the relative angle  $\theta$  from  $\pi/2$  to 0, a transition from the weak light-matter coupling to strong coupling regimes can be observed (Figure 7b,c, and see simulation details in Methods). Furthermore, combining room-temperature polariton condensation and superfluid phenomena in perovskites<sup>196,205</sup> with the ultralow condensation threshold with BIC structures<sup>75</sup> could significantly improve device performance, offering a distinct opportunity to develop electrically pumped polariton condensation and lasers in perovskite.<sup>206</sup>

Because 2D AFM excitons can exhibit long-range spin ordering and magnons, exciton polaritons could exhibit more unconventional quantum phenomena and attractive optoelectronic devices by taking advantages of the nonreciprocity of magnons and exploring their excitonic coupling with magnons under the external magnetic field.

From a photonics perspective, we also expect rapid advancements in exciton polaritons by integrating various emerging photonic nanostructures with topological properties. Previously demonstrated exciton polaritons integrated with topological photonic crystals were mainly based on quantum spin Hall topological PCs.<sup>34,35</sup> The supported edge states in this configuration naturally exhibit significant out-of-plane radiation loss, which greatly hinders the realization of polariton condensation and quantum superfluids with long propagation lengths. By considering other topological structures, such as quantum valley Hall PC,<sup>207,208</sup> high-order PC of corner states,<sup>209</sup> and recently realized topological Dirac-vortex states,<sup>210,211</sup> the optical performance can be significantly enhanced and topological polariton condensations with a lower threshold may be achieved with fascinating topological nature. Taking valley Hall PCs as a representative example of various photonic topological insulator schemes, Figure 7d shows a conceptual illustration of a valley Hall photonic crystal slab integrated with emerging 2D excitonic materials. This photonic crystal slab can support topological edge states at the domain wall between two regions with opposite topological charges (Figure 7e and more simulation details in Methods). As shown in Figure 7f, there are gapless polaritonic states within the bulk polariton bandgaps (gray shaded regions and see details in Methods). These topological polariton edge states are not only robust against sharp bends at the nanoscale but also have negligible radiation loss in free space. By winding the boundary into a closed-loop triangular ring, we can create discrete whispering-gallery modes inside the bulk bandgap, with modal profiles tightly bonded to the boundary (Figure 7g and see details in Methods), without observable back reflection around sharp bends.

By fully leveraging the attractive properties from both 2D semiconductors and photonic nanostructures, we prospect that exciton polariton systems will provide an exciting platform for experimentally exploring fascinating topological physics with strong bosonic interactions and many-body physics. Considering the recent advancements in 2D exciton systems such as 2D semiconductor moiré superlattices, we optimistically predict the experimental realizations of topological polariton solitons,<sup>212</sup> topological Bose–Hubbard lattices,<sup>213</sup> and topological photon blockades<sup>26</sup> based on the exciton polaritons in the future. This development could significantly impact our understanding of polariton physics and further enhance the potential applications of low-threshold coherent light sources and nonlinear optics.

## METHODS

In our outlook on 2D exciton polaritons, numerical simulations of angle-resolved reflection spectra are calculated by finite-difference-time-domain method. We assume the dielectric functions of 2D semiconductor material as a Lorentz model to obtain weak and strong coupling dispersions in Figure 7b,c:

$\epsilon = \epsilon_0 + \frac{\omega_p^2}{\omega_0^2 - \omega^2 - i\gamma\omega}$ . The specific Lorentz model parameters depend on different materials, as well as temperatures. For instance, 2DPKs can operate at room temperature while 2D

AFMs only exhibit relatively narrow exciton line width at temperature below Neel temperature  $T_N$ . In Figure 7b,c, we adopted background permittivity of  $\epsilon_0 = 11$ , line width of  $\gamma = 6.6$  meV, and exciton resonant energy of  $\omega_0 = 1.975$  eV for a simulation example. We have also used a tight-binding approximation to theoretically calculate the band diagrams and spatial distributions of topological exciton polaritons in Figure 7f,g. Specifically, we consider a honeycomb photonic lattice, where each sublattice (labeled by  $s = 1, 2$ ) of the  $i$ -th unit cell contains a photonic mode  $a_{s,i}$  and an excitonic mode  $b_{s,i}$ . The entire Hamiltonian of the light-matter coupled system is

$$H/\hbar = \sum_{s,i} [\omega_{\text{ph}} + (-1)^s \cdot \delta] \cdot a_{s,i}^\dagger a_{s,i} - \sum_{s,s',i,i'} \kappa \cdot (a_{s,i}^\dagger a_{s',i'} + a_{s,i} a_{s',i'}^\dagger) + \sum_{s,i} \omega_{\text{ex}} \cdot b_{s,i}^\dagger b_{s,i} - \sum_{s,i} g \cdot (a_{s,i}^\dagger b_{s,i} + a_{s,i} b_{s,i}^\dagger) \quad (8)$$

Here, the first and second terms on the right-hand side of eq 8 represent the pure photonic topological Hamiltonians with on-site frequency modulation  $\delta$  and the nearest photonic mode coupling coefficient  $\kappa$ . The third term represents the collective excitonic modes, and the last term describes the light-matter coupling. We solve the eigenvalue problem of this Hamiltonian in momentum space to obtain exciton-polariton valley edge state dispersion in Figure 7f, and in real space to obtain the spatial distribution of excitons in Figure 7g.

## AUTHOR INFORMATION

### Corresponding Authors

**Jingwen Ma** – Faculty of Science and Engineering, The University of Hong Kong, Hong Kong, SAR, P. R. China; Email: [jwma@hku.hk](mailto:jwma@hku.hk)

**Xiang Zhang** – Faculty of Science and Engineering, The University of Hong Kong, Hong Kong, SAR, P. R. China; Department of Physics, The University of Hong Kong, Hong Kong, SAR, P. R. China; Email: [president@hku.hk](mailto:president@hku.hk)

**Xiaoze Liu** – Key Laboratory of Artificial Micro/Nano Structure of Ministry of Education, School of Physics and Technology, Wuhan University, Wuhan 430072, P. R. China; Wuhan Institute of Quantum Technology, Wuhan 430206, P. R. China; Wuhan University Shenzhen Research Institute, Shenzhen 518057, P. R. China; [orcid.org/0000-0002-3586-6408](https://orcid.org/0000-0002-3586-6408); Email: [xiaozeliu@whu.edu.cn](mailto:xiaozeliu@whu.edu.cn)

### Authors

**Haifeng Kang** – Key Laboratory of Artificial Micro/Nano Structure of Ministry of Education, School of Physics and Technology, Wuhan University, Wuhan 430072, P. R. China

**Junyu Li** – Key Laboratory of Artificial Micro/Nano Structure of Ministry of Education, School of Physics and Technology, Wuhan University, Wuhan 430072, P. R. China

Complete contact information is available at:

<https://pubs.acs.org/10.1021/acsnano.3c07993>

### Author Contributions

The manuscript was written through contributions of all authors. All authors have given approval to the final version of the manuscript.

### Funding

This work was supported by the National Natural Science Foundation of China (62005202, 12074297, 62261160386), the Fundamental Research Funds for the Central Universities

(No. 2042023kf0195), Guangdong Basic and Applied Basic Research Foundation (No. 2023A1515011222), and by Research Grants Council, University Grants Committee of Hong Kong (N\_HKU750/22).

## Notes

The authors declare no competing financial interest.

## REFERENCES

- (1) Weisbuch, C.; Nishioka, M.; Ishikawa, A.; Arakawa, Y. Observation of the Coupled Exciton-Photon Mode Splitting in a Semiconductor Quantum Microcavity. *Phys. Rev. Lett.* **1992**, *69*, 3314–3317.
- (2) Deng, H.; Haug, H.; Yamamoto, Y. Exciton-Polariton Bose–Einstein Condensation. *Rev. Mod. Phys.* **2010**, *82*, 1489–1537.
- (3) Sanvitto, D.; Kéna-Cohen, S. The Road towards Polaritonic Devices. *Nat. Mater.* **2016**, *15*, 1061–1073.
- (4) Schneider, C.; Winkler, K.; Fraser, M. D.; Kamp, M.; Yamamoto, Y.; Ostrovskaya, E. A.; Höfling, S. Exciton-Polariton Trapping and Potential Landscape Engineering. *Rep. Prog. Phys.* **2017**, *80*, No. 016503.
- (5) Ghosh, S.; Su, R.; Zhao, J.; Fieramosca, A.; Wu, J.; Li, T.; Zhang, Q.; Li, F.; Chen, Z.; Liew, T.; Sanvitto, D.; Xiong, Q. Microcavity Exciton Polaritons at Room Temperature. *Photonics Insights* **2022**, *1*, R04.
- (6) Luo, S.; Zhou, H.; Zhang, L.; Chen, Z. Nanophotonics of Microcavity Exciton–Polaritons. *Appl. Phys. Rev.* **2023**, *10*, No. 011316.
- (7) Byrnes, T.; Kim, N. Y.; Yamamoto, Y. Exciton-Polariton Condensates. *Nat. Phys.* **2014**, *10*, 803–813.
- (8) Schneider, C.; Glazov, M. M.; Korn, T.; Höfling, S.; Urbaszek, B. Two-Dimensional Semiconductors in the Regime of Strong Light-Matter Coupling. *Nat. Commun.* **2018**, *9*, 2695.
- (9) Su, R.; Fieramosca, A.; Zhang, Q.; Nguyen, H. S.; Deleporte, E.; Chen, Z.; Sanvitto, D.; Liew, T. C. H.; Xiong, Q. Perovskite Semiconductors for Room-Temperature Exciton-Polaritons. *Nat. Mater.* **2021**, *20*, 1315–1324.
- (10) Nalitov, A. V.; Solnyshkov, D. D.; Malpuech, G. Polariton Z Topological Insulator. *Phys. Rev. Lett.* **2015**, *114*, No. 116401.
- (11) Lu, L.; Joannopoulos, J. D.; Soljačić, M. Topological Photonics. *Nat. Photonics* **2014**, *8*, 821–829.
- (12) Ozawa, T.; Price, H. M.; Amo, A.; Goldman, N.; Hafezi, M.; Lu, L.; Rechtsman, M. C.; Schuster, D.; Simon, J.; Zilberberg, O.; Carusotto, I. Topological Photonics. *Rev. Mod. Phys.* **2019**, *91*, 15006.
- (13) Khanikaev, A. B.; Shvets, G. Two-Dimensional Topological Photonics. *Nat. Photonics* **2017**, *11*, 763–773.
- (14) Smirnova, D.; Leykam, D.; Chong, Y.; Kivshar, Y. Nonlinear Topological Photonics. *Appl. Phys. Rev.* **2020**, *7*, No. 021306.
- (15) Karzig, T.; Bardyn, C.; Lindner, N. H.; Refael, G. Topological Polaritons. *Phys. Rev. X* **2015**, *5*, No. 031001.
- (16) Deng, H.; Weihs, G.; Santori, C.; Bloch, J.; Yamamoto, Y. Condensation of Semiconductor Microcavity Exciton Polaritons. *Science* **2002**, *298*, 199–202.
- (17) Kasprzak, J.; Richard, M.; Kundermann, S.; Baas, A.; Jeambrun, P.; Keeling, J. M. J.; Marchetti, F. M.; Szymánska, M. H.; André, R.; Staehli, J. L.; Savona, V.; Littlewood, P. B.; Deveaud, B.; Dang, L. S. Bose–Einstein Condensation of Exciton Polaritons. *Nature* **2006**, *443*, 409–414.
- (18) Balili, R.; Hartwell, V.; Snoke, D.; Pfeiffer, L.; West, K. Bose–Einstein Condensation of Microcavity Polaritons in a Trap. *Science* **2007**, *316*, 1007–1011.
- (19) Amo, A.; Lefrère, J.; Pigeon, S.; Adrados, C.; Ciuti, C.; Carusotto, I.; Houdré, R.; Giacobino, E.; Bramati, A. Superfluidity of Polaritons in Semiconductor Microcavities. *Nat. Phys.* **2009**, *5*, 805–810.
- (20) Amo, A.; Sanvitto, D.; Laussy, F. P.; Ballarini, D.; del Valle, E.; Martin, M. D.; Lemaître, A.; Bloch, J.; Krizhanovskii, D. N.; Skolnick, M. S.; Tejedor, C.; Viña, L. Collective Fluid Dynamics of a Polariton Condensate in a Semiconductor Microcavity. *Nature* **2009**, *457*, 291–295.
- (21) Lerario, G.; Fieramosca, A.; Barachati, F.; Ballarini, D.; Daskalakis, K. S.; Dominici, L.; De Giorgi, M.; Maier, S. A.; Gigli, G.; Kéna-Cohen, S.; Sanvitto, D. Room-Temperature Superfluidity in a Polariton Condensate. *Nat. Phys.* **2017**, *13*, 837–841.
- (22) Carusotto, I.; Ciuti, C. Quantum Fluids of Light. *Rev. Mod. Phys.* **2013**, *85*, 299–366.
- (23) Lodahl, P.; Mahmoodian, S.; Stobbe, S. Interfacing Single Photons and Single Quantum Dots with Photonic Nanostructures. *Rev. Mod. Phys.* **2015**, *87*, 347–400.
- (24) Müller, K.; Rundquist, A.; Fischer, K. A.; Sarmiento, T.; Lagoudakis, K. G.; Kelaita, Y. A.; Sánchez Muñoz, C.; Del Valle, E.; Laussy, F. P.; Vučković, J. Coherent Generation of Nonclassical Light on Chip via Detuned Photon Blockade. *Phys. Rev. Lett.* **2015**, *114*, No. 233601.
- (25) Müller, K.; Fischer, K. A.; Rundquist, A.; Dory, C.; Lagoudakis, K. G.; Sarmiento, T.; Kelaita, Y. A.; Borish, V.; Vučković, J. Ultrafast Polariton-Phonon Dynamics of Strongly Coupled Quantum Dot-Nanocavity Systems. *Phys. Rev. X* **2015**, *5*, No. 031006.
- (26) Delteil, A.; Fink, T.; Schade, A.; Hofling, S.; Schneider, C.; Imamoglu, A. Towards Polariton Blockade of Confined Exciton–Polaritons. *Nat. Mater.* **2019**, *18*, 219–222.
- (27) Muñoz-matutano, G.; Wood, A.; Johnsson, M.; Vidal, X.; Baragiola, B. Q.; Reinhard, A.; Lemaître, A.; Bloch, J.; Amo, A.; Nogues, G.; Besga, B.; Richard, M.; Volz, T. Emergence of Quantum Correlations from Interacting Fibre-Cavity Polaritons. *Nat. Mater.* **2019**, *18*, 213.
- (28) Whittaker, C. E.; Dzurnak, B.; Egorov, O. A.; Buonaiuto, G.; Walker, P. M.; Cancellieri, E.; Whittaker, D. M.; Clarke, E.; Gavrilov, S. S.; Skolnick, M. S.; Krizhanovskii, D. N. Polariton Pattern Formation and Photon Statistics of the Associated Emission. *Phys. Rev. X* **2017**, *7*, No. 031033.
- (29) Togan, E.; Lim, H.; Faelt, S.; Wegscheider, W.; Imamoglu, A. Enhanced Interactions between Dipolar Polaritons. *Phys. Rev. Lett.* **2018**, *121*, No. 227402.
- (30) Orfanakis, K.; Rajendran, S. K.; Walther, V.; Volz, T.; Pohl, T.; Ohadi, H. Rydberg Exciton–Polaritons in a Cu<sub>2</sub>O Microcavity. *Nat. Mater.* **2022**, *21*, 767–772.
- (31) Snijders, H. J.; Frey, J. A.; Norman, J.; Flayac, H.; Savona, V.; Gossard, A. C.; Bowers, J. E.; van Exter, M. P.; Bouwmeester, D.; Löffler, W. Observation of the Unconventional Photon Blockade. *Phys. Rev. Lett.* **2018**, *121*, No. 043601.
- (32) Englund, D.; Faraon, A.; Fushman, I.; Stoltz, N.; Petroff, P.; Vučković, J. Controlling Cavity Reflectivity with a Single Quantum Dot. *Nature* **2007**, *450*, 857–861.
- (33) Klemmt, S.; Harder, T. H.; Egorov, O. A.; Winkler, K.; Ge, R.; Bandres, M. A.; Emmerling, M.; Worschech, L.; Liew, T. C. H.; Segev, M.; Schneider, C.; Hofling, S. Exciton-Polariton Topological Insulator. *Nature* **2018**, *562*, 552–556.
- (34) Liu, W.; Ji, Z.; Wang, Y.; Modi, G.; Hwang, M.; Zheng, B.; Sorger, V. J.; Pan, A.; Agarwal, R. Generation of Helical Topological Exciton-Polaritons. *Science* **2020**, *370*, 600–604.
- (35) Li, M.; Sinev, I.; Benimetskiy, F.; Ivanova, T.; Khestanova, E.; Kiriushchikina, S.; Vakulenko, A.; Guddala, S.; Skolnick, M.; Menon, V. M.; Krizhanovskii, D.; Alù, A.; Samusev, A.; Khanikaev, A. B. Experimental Observation of Topological Z<sub>2</sub> Exciton-Polaritons in Transition Metal Dichalcogenide Monolayers. *Nat. Commun.* **2021**, *12*, 4425.
- (36) Knox, R. S. *Theory of Excitons*; Academic Press, 1963.
- (37) Agranovich, V. M.; Gartstein, Yu. N.; Litinskaya, M. Hybrid Resonant Organic-Inorganic Nanostructures for Optoelectronic Applications. *Chem. Rev.* **2011**, *111*, 5179–5214.
- (38) Wang, G.; Chernikov, A.; Glazov, M. M.; Heinz, T. F.; Marie, X.; Amand, T.; Urbaszek, B. Excitons in Atomically Thin Transition Metal Dichalcogenides. *Rev. Mod. Phys.* **2018**, *90*, 21001.
- (39) Xiao, J.; Zhao, M.; Wang, Y.; Zhang, X. Excitons in Atomically Thin 2D Semiconductors and Their Applications. *Nanophotonics* **2017**, *6*, 1309–1328.

- (40) Agranovich, V. M.; Basko, D. M.; Rocca, G. C. L.; Bassani, F. Excitons and Optical Nonlinearities in Hybrid Organic-Inorganic Nanostructures. *J. Phys.: Condens. Matter* **1998**, *10*, 9369.
- (41) Frenkel, J. On the Transformation of Light into Heat in Solids. *Phys. Rev.* **1931**, *37*, 17–44.
- (42) Wannier, G. H. The Structure of Electronic Excitation Levels in Insulating Crystals. *Phys. Rev.* **1937**, *52*, 191–197.
- (43) Mak, K. F.; Lee, C.; Hone, J.; Shan, J.; Heinz, T. F. Atomically Thin MoS<sub>2</sub>: A New Direct-Gap Semiconductor. *Phys. Rev. Lett.* **2010**, *105*, No. 136805.
- (44) Splendiani, A.; Sun, L.; Zhang, Y.; Li, T.; Kim, J.; Chim, C.-Y.; Galli, G.; Wang, F. Emerging Photoluminescence in Monolayer MoS<sub>2</sub>. *Nano Lett.* **2010**, *10*, 1271–1275.
- (45) Wilson, N. P.; Yao, W.; Shan, J.; Xu, X. Excitons and Emergent Quantum Phenomena in Stacked 2D Semiconductors. *Nature* **2021**, *599*, 383–392.
- (46) Huang, D.; Choi, J.; Shih, C. K.; Li, X. Excitons in Semiconductor Moiré Superlattices. *Nat. Nanotechnol.* **2022**, *17*, 227–238.
- (47) Blancon, J. C.; Stier, A. V.; Tsai, H.; Nie, W.; Stoumpos, C. C.; Traoré, B.; Pedesseau, L.; Kepenekian, M.; Katsutani, F.; Noe, G. T.; Kono, J.; Tretiak, S.; Crooker, S. A.; Katan, C.; Kanatzidis, M. G.; Crochet, J. J.; Even, J.; Mohite, A. D. Scaling Law for Excitons in 2D Perovskite Quantum Wells. *Nat. Commun.* **2018**, *9*, 2254.
- (48) Blancon, J.; Even, J.; Stoumpos, C. C.; Kanatzidis, M. G.; Mohite, A. D. Semiconductor Physics of Organic–Inorganic 2D Halide Perovskites. *Nat. Nanotechnol.* **2020**, *15*, 969–985.
- (49) Kang, S.; Kim, K.; Kim, B. H.; Kim, J.; Sim, K. I.; Lee, J. U.; Lee, S.; Park, K.; Yun, S.; Kim, T.; Nag, A.; Walters, A.; Garcia-Fernandez, M.; Li, J.; Chapon, L.; Zhou, K. J.; Son, Y. W.; Kim, J. H.; Cheong, H.; Park, J. G. Coherent Many-Body Exciton in van Der Waals Antiferromagnet NiPS<sub>3</sub>. *Nature* **2020**, *583*, 785–789.
- (50) Wilson, N. E. C.; Lee, K.; Cenker, J.; Xie, K.; Dismukes, A. H.; Telford, E. J.; Fonseca, J.; Sivakumar, S.; Dean, C.; Cao, T.; Roy, X.; Xu, X.; Zhu, X. Interlayer Electronic Coupling on Demand in a 2D Magnetic Semiconductor. *Nat. Mater.* **2021**, *20*, 1657–1662.
- (51) Shen, F.; Zhang, Z.; Zhou, Y.; Ma, J.; Chen, K.; Chen, H.; Wang, S.; Xu, J.; Chen, Z. Transition Metal Dichalcogenide Metaphotonic and Self-Coupled Polaritonic Platform Grown by Chemical Vapor Deposition. *Nat. Commun.* **2022**, *13*, 5597.
- (52) He, K.; Kumar, N.; Zhao, L.; Wang, Z.; Mak, K. F.; Zhao, H.; Shan, J. Tightly Bound Excitons in Monolayer WSe<sub>2</sub>. *Phys. Rev. Lett.* **2014**, *113*, No. 026803.
- (53) Mak, K. F.; He, K.; Lee, C.; Lee, G. H.; Hone, J.; Heinz, T. F.; Shan, J. Tightly Bound Trions in Monolayer MoS<sub>2</sub>. *Nat. Mater.* **2013**, *12*, 207–211.
- (54) Ye, Z.; Cao, T.; O'Brien, K.; Zhu, H.; Yin, X.; Wang, Y.; Louie, S. G.; Zhang, X. Probing Excitonic Dark States in Single-Layer Tungsten Disulphide. *Nature* **2014**, *513*, 214–218.
- (55) Chernikov, A.; Berkelbach, T. C.; Hill, H. M.; Rigosi, A.; Li, Y.; Aslan, O. B.; Reichman, D. R.; Hybertsen, M. S.; Heinz, T. F. Exciton Binding Energy and Nonhydrogenic Rydberg Series in Monolayer WS<sub>2</sub>. *Phys. Rev. Lett.* **2014**, *113*, No. 076802.
- (56) Liu, X.; Galfsky, T.; Sun, Z.; Xia, F.; Lin, E.; Lee, Y.-H.; Kéna-Cohen, S.; Menon, V. M. Strong Light–Matter Coupling in Two-Dimensional Atomic Crystals. *Nat. Photonics* **2015**, *9*, 30–34.
- (57) Fieramosca, A.; Polimeno, L.; Ardizzone, V.; De Marco, L.; Pugliese, M.; Maiorano, V.; De Giorgi, M.; Dominici, L.; Gigli, G.; Gerace, D.; Ballarini, D.; Sanvitto, D. Two-Dimensional Hybrid Perovskites Sustaining Strong Polariton Interactions at Room Temperature. *Sci. Adv.* **2019**, *5*, No. eaav9967.
- (58) Dirnberger, F.; Bushati, R.; Datta, B.; Kumar, A.; MacDonald, A. H.; Baldini, E.; Menon, V. M. Spin-Correlated Exciton–Polaritons in a van Der Waals Magnet. *Nat. Nanotechnol.* **2022**, *17*, 1060–1064.
- (59) Dirnberger, F.; Quan, J.; Bushati, R.; Diederich, G. M.; Florian, M.; Klein, J.; Mosina, K.; Sofer, Z.; Xu, X.; Kamra, A.; García-Vidal, F. J.; Alù, A.; Menon, V. M. Magneto-Optics in a van Der Waals Magnet Tuned by Self-Hybridized Polaritons. *Nature* **2023**, *620*, 533–537.
- (60) Wang, T.; Zhang, D.; Yang, S.; Lin, Z.; Chen, Q.; Yang, J.; Gong, Q.; Chen, Z.; Ye, Y.; Liu, W. Magnetically-Dressed CrSBr Exciton-Polaritons in Ultrastrong Coupling Regime. *Nat. Commun.* **2023**, *14*, 5966.
- (61) Vahala, K. J. Optical Microcavities. *Nature* **2003**, *424*, 839–846.
- (62) Chikkaraddy, R.; de Nijs, B.; Benz, F.; Barrow, S. J.; Scherman, O. A.; Rosta, E.; Demetriadou, A.; Fox, P.; Hess, O.; Baumberg, J. J. Single-Molecule Strong Coupling at Room Temperature in Plasmonic Nanocavities. *Nature* **2016**, *535*, 127–130.
- (63) Sun, Y.; Yoon, Y.; Steger, M.; Liu, G.; Pfeiffer, L. N.; West, K.; Snoko, D. W.; Nelson, K. A. Direct Measurement of Polariton-Polariton Interaction Strength. *Nat. Phys.* **2017**, *13*, 870–875.
- (64) Hsu, C. W.; Zhen, B.; Stone, A. D.; Joannopoulos, J. D.; Soljačić, M. Bound States in the Continuum. *Nat. Rev. Mater.* **2016**, *1*, 16048.
- (65) Zhang, L.; Gogna, R.; Burg, W.; Tutuc, E.; Deng, H. Photonic-Crystal Exciton-Polaritons in Monolayer Semiconductors. *Nat. Commun.* **2018**, *9*, 713.
- (66) Goldberg, D.; Deych, L. I.; Lisyansky, A. A.; Shi, Z.; Menon, V. M.; Tokranov, V.; Yakimov, M.; Oktyabrsky, S. Exciton-Lattice Polaritons in Multiple-Quantum-Well-Based Photonic Crystals. *Nat. Photonics* **2009**, *3*, 662–666.
- (67) Yoshie, T.; Scherer, A.; Hendrickson, J.; Khitrova, G.; Gibbs, H. M.; Rupper, G.; Ell, C.; Shchekin, O. B.; Deppe, D. G. Vacuum Rabi Splitting with a Single Quantum Dot in a Photonic Crystal Nanocavity. *Nature* **2004**, *432*, 200–203.
- (68) Zhang, Z.; Qiao, X.; Midya, B.; Liu, K.; Sun, J.; Wu, T.; Liu, W.; Agarwal, R.; Jornet, J. M.; Longhi, S.; Litchinitser, N. M.; Feng, L. Tunable Topological Charge Vortex Microlaser. *Science* **2020**, *368*, 760–763.
- (69) Barik, S.; Karasahin, A.; Flower, C.; Cai, T.; Miyake, H.; Degottardi, W.; Hafezi, M.; Waks, E. A Topological Quantum Optics Interface. *Science* **2018**, *359*, 666–668.
- (70) Maggolini, E.; Polimeno, L.; Todisco, F.; Di Renzo, A.; Han, B.; De Giorgi, M.; Ardizzone, V.; Schneider, C.; Mastria, R.; Cannavale, A.; Pugliese, M.; De Marco, L.; Rizzo, A.; Maiorano, V.; Gigli, G.; Gerace, D.; Sanvitto, D.; Ballarini, D. Strongly Enhanced Light–Matter Coupling of Monolayer WS<sub>2</sub> from a Bound State in the Continuum. *Nat. Mater.* **2023**, *22*, 964–969.
- (71) St-Jean, P.; Goblot, V.; Galopin, E.; Lemaître, A.; Ozawa, T.; Le Gratiet, L.; Sagnes, I.; Bloch, J.; Amo, A. Lasing in Topological Edge States of a One-Dimensional Lattice. *Nat. Photonics* **2017**, *11*, 651–656.
- (72) Su, R.; Ghosh, S.; Liew, T. C. H.; Xiong, Q. Optical Switching of Topological Polariton Phase in a Perovskite Lattice. *Sci. Adv.* **2021**, *7*, No. eabf8049.
- (73) Dusel, M.; Betzold, S.; Egorov, O. A.; Klemmt, S.; Ohmer, J.; Fischer, U.; Höfling, S.; Schneider, C. Room Temperature Organic Exciton–Polariton Condensate in a Lattice. *Nat. Commun.* **2020**, *11*, 1–7.
- (74) Kravtsov, V.; Khestanova, E.; Benimetskiy, F. A.; Ivanova, T.; Samusev, A. K.; Sinev, I. S.; Pidgayko, D.; Mozharov, A. M.; Mukhin, I. S.; Lozhkin, M. S.; Kapitonov, Y. V.; Brichkin, A. S.; Kulakovskii, V. D.; Shelykh, I. A.; Tartakovskii, A. I.; Walker, P. M.; Skolnick, M. S.; Krizhanovskii, D. N.; Iorsh, I. V. Nonlinear Polaritons in a Monolayer Semiconductor Coupled to Optical Bound States in the Continuum. *Light Sci. Appl.* **2020**, *9*, 56.
- (75) Ardizzone, V.; Riminucci, F.; Zanotti, S.; Gianfrate, A.; Efthymiou-Tsirioni, M.; Suarez-Forero, D. G.; Todisco, F.; De Giorgi, M.; Trypogeorgos, D.; Gigli, G.; Baldwin, K.; Pfeiffer, L.; Ballarini, D.; Nguyen, H. S.; Gerace, D.; Sanvitto, D. Polariton Bose–Einstein Condensate from a Bound State in the Continuum. *Nature* **2022**, *605*, 447–452.
- (76) Baumberg, J. J.; Aizpurua, J.; Mikkelsen, M. H.; Smith, D. R. Extreme Nanophotonics from Ultrathin Metallic Gaps. *Nat. Mater.* **2019**, *18*, 668–678.
- (77) Akselrod, G. M.; Argyropoulos, C.; Hoang, T. B.; Ciraci, C.; Fang, C.; Huang, J.; Smith, D. R.; Mikkelsen, M. H. Probing the

Mechanisms of Large Purcell Enhancement in Plasmonic Nano-antennas. *Nat. Photonics* **2014**, *8*, 835–840.

(78) Ciraci, C.; Hill, R. T.; Mock, J. J.; Urzhumov, Y.; Fernández-Domínguez, A. I.; Maier, S. A.; Pendry, J. B.; Chilkoti, A.; Smith, D. R. Probing the Ultimate Limits of Plasmonic Enhancement. *Science* **2012**, *337*, 1072–1074.

(79) Benz, F.; Schmidt, M. K.; Dreismann, A.; Chikkaraddy, R.; Zhang, Y.; Demetriadou, A.; Carnegie, C.; Ohadi, H.; de Nijs, B.; Esteban, R.; Aizpurua, J.; Baumberg, J. J. Single-Molecule Optomechanics in “Picocavities. *Science* **2016**, *354*, 726–729.

(80) Li, W.; Zhou, Q.; Zhang, P.; Chen, X.-W. Bright Optical Eigenmode of Inm3Mode Volume. *Phys. Rev. Lett.* **2021**, *126*, No. 257401.

(81) Wang, S.; Li, S.; Chervy, T.; Shalabney, A.; Azzini, S.; Orgiu, E.; Hutchison, J. A.; Genet, C.; Samorì, P.; Ebbesen, T. W. Coherent Coupling of WS<sub>2</sub> Monolayers with Metallic Photonic Nanostructures at Room Temperature. *Nano Lett.* **2016**, *16*, 4368–4374.

(82) Liu, W.; Lee, B.; Naylor, C. H.; Ee, H.-S.; Park, J.; Johnson, A. T. C.; Agarwal, R. Strong Exciton-Plasmon Coupling in MoS<sub>2</sub> Coupled with Plasmonic Lattice. *Nano Lett.* **2016**, *16*, 1262–1269.

(83) Hakala, T. K.; Moilanen, A. J.; Väkeväinen, A. I.; Guo, R.; Martikainen, J. P.; Daskalakis, K. S.; Rekola, H. T.; Julku, A.; Törmä, P. Bose–Einstein Condensation in a Plasmonic Lattice. *Nat. Phys.* **2018**, *14*, 739–744.

(84) Savona, V.; Andreani, L. C.; Schwendimann, P.; Quattropani, A. Quantum Well Excitons in Semiconductor Microcavities: Unified Treatment of Weak and Strong Coupling Regimes. *Solid State Commun.* **1995**, *93*, 733–739.

(85) Houdré, R. Early Stages of Continuous Wave Experiments on Cavity-Polaritons. *Phys. Status Solidi B* **2005**, *242*, 2167–2196.

(86) Liu, X.; Bao, W.; Li, Q.; Ropp, C.; Wang, Y.; Zhang, X. Control of Coherently Coupled Exciton Polaritons in Monolayer Tungsten Disulfide. *Phys. Rev. Lett.* **2017**, *119*, No. 027403.

(87) Hennessy, K.; Badolato, A.; Winger, M.; Gerace, D.; Atatüre, M.; Gulde, S.; Fält, S.; Hu, E. L.; Imamoglu, A. Quantum Nature of a Strongly Coupled Single Quantum Dot–Cavity System. *Nature* **2007**, *445*, 896–899.

(88) Lidzey, D. G.; Bradley, D. D. C.; Skolnick, M. S.; Virgili, T.; Walker, S.; Whittaker, D. M. Strong Exciton–Photon Coupling in an Organic Semiconductor Microcavity. *Nature* **1998**, *395*, 53–55.

(89) Fujita, T.; Sato, Y.; Kuitani, T.; Ishihara, T. Tunable Polariton Absorption of Distributed Feedback Microcavities at Room Temperature. *Phys. Rev. B - Condens. Matter Mater. Phys.* **1998**, *57*, 12428–12434.

(90) Reithmaier, J. P.; Sek, G.; Löffler, a; Hofmann, C.; Kuhn, S.; Reitzenstein, S.; Keldysh, L. V.; Kulakovskii, V. D.; Reinecke, T. L.; Forchel, a. Strong Coupling in a Single Quantum Dot-Semiconductor Microcavity System. *Nature* **2004**, *432*, 197–200.

(91) Berloff, N. G.; Silva, M.; Kalinin, K.; Askitopoulos, A.; Töpfer, J. D.; Cilibrizzi, P.; Langbein, W.; Lagoudakis, P. G. Realizing the Classical XY Hamiltonian in Polariton Simulators. *Nat. Mater.* **2017**, *16*, 1120–1126.

(92) Tao, R.; Peng, K.; Haeberlé, L.; Li, Q.; Jin, D.; Fleming, G. R.; Kéna-Cohen, S.; Zhang, X.; Bao, W. Halide Perovskites Enable Polaritonic XY Spin Hamiltonian at Room Temperature. *Nat. Mater.* **2022**, *21*, 761–766.

(93) Kim, N. Y.; Yamamoto, Y. Exciton-Polariton Quantum Simulators. In *Quantum Simulations with Photons and Polaritons: Merging Quantum Optics with Condensed Matter Physics*; Angelakis, D. G., Ed.; Springer International Publishing: Cham, 2017; pp 91–121.

(94) Schneider, C.; Rahimi-Iman, A.; Kim, N. Y.; Fischer, J.; Savenko, I. G.; Amthor, M.; Lermer, M.; Wolf, A.; Worschech, L.; Kulakovskii, V. D.; Shelykh, I. a; Kamp, M.; Reitzenstein, S.; Forchel, A.; Yamamoto, Y.; Höfling, S. An Electrically Pumped Polariton Laser. *Nature* **2013**, *497*, 348–352.

(95) Bhattacharya, P.; Xiao, B.; Das, A.; Bhowmick, S.; Heo, J. Solid State Electrically Injected Exciton-Polariton Laser. *Phys. Rev. Lett.* **2013**, *110*, No. 206403.

(96) Bhattacharya, P.; Frost, T.; Deshpande, S.; Baten, M. Z.; Hazari, A.; Das, A. Room Temperature Electrically Injected Polariton Laser. *Phys. Rev. Lett.* **2014**, *112*, No. 236802.

(97) Sun, L.; Chen, Z.; Ren, Q.; Yu, K.; Bai, L.; Zhou, W.; Xiong, H.; Zhu, Z. Q.; Shen, X. Direct Observation of Whispering Gallery Mode Polaritons and Their Dispersion in a ZnO Tapered Microcavity. *Phys. Rev. Lett.* **2008**, *100*, No. 156403.

(98) Lai, Y.-Y.; Lan, Y.-P.; Lu, T.-C. Strong Light–Matter Interaction in ZnO Microcavities. *Light Sci. Appl.* **2013**, *2*, e76–e76.

(99) Christopoulos, S.; Von Högersthal, G. B. H.; Grundy, A. J. D.; Lagoudakis, P. G.; Kavokin, A. V.; Baumberg, J. J.; Christmann, G.; Butté, R.; Feltn, E.; Carlin, J.-F.; Grandjean, N. Room-Temperature Polariton Lasing in Semiconductor Microcavities. *Phys. Rev. Lett.* **2007**, *98*, No. 126405.

(100) Hutchison, J. A.; Schwartz, T.; Genet, C.; Devaux, E.; Ebbesen, T. W. Modifying Chemical Landscapes by Coupling to Vacuum Fields. *Angew. Chem., Int. Ed.* **2012**, *51*, 1592–1596.

(101) Thomas, A.; Lethuillier-Karl, L.; Nagarajan, K.; Vergauwe, R. M. A.; George, J.; Chervy, T.; Shalabney, A.; Devaux, E.; Genet, C.; Moran, J.; Ebbesen, T. W. Tilting a Ground-State Reactivity Landscape by Vibrational Strong Coupling. *Science* **2019**, *363*, 615–619.

(102) Sidler, D.; Schäfer, C.; Ruggenthaler, M.; Rubio, A. Polaritonic Chemistry: Collective Strong Coupling Implies Strong Local Modification of Chemical Properties. *J. Phys. Chem. Lett.* **2021**, *12*, 508–516.

(103) Sun, Z.; Gu, J.; Ghazaryan, A.; Shotan, Z.; Considine, C. R.; Dollar, M.; Chakraborty, B.; Liu, X.; Ghaemi, P.; Kéna-Cohen, S.; Menon, V. M. Optical Control of Room-Temperature Valley Polaritons. *Nat. Photonics* **2017**, *11*, 491–496.

(104) Chen, Y.-J.; Cain, J. D.; Stanev, T. K.; Dravid, V. P.; Stern, N. P. Valley-Polarized Exciton-Polaritons in a Monolayer Semiconductor. *Nat. Photonics* **2017**, *11*, 431–435.

(105) Dufferwiel, S.; Lyons, T. P.; Solnyshkov, D. D.; Trichet, A. A. P.; Withers, F.; Schwarz, S.; Malpuech, G.; Smith, J. M.; Novoselov, K. S.; Skolnick, M. S.; Krizhanovskii, D. N.; Tartakovskii, A. I. Valley Addressable Exciton-Polaritons in Atomically Thin Semiconductors. *Nat. Photonics* **2017**, *11*, 497–501.

(106) Dufferwiel, S.; Lyons, T. P.; Solnyshkov, D. D.; Trichet, A. A. P.; Catanzaro, A.; Withers, F.; Malpuech, G.; Smith, J. M.; Novoselov, K. S.; Skolnick, M. S.; Krizhanovskii, D. N.; Tartakovskii, A. I. Valley Coherent Exciton-Polaritons in a Monolayer Semiconductor. *Nat. Commun.* **2018**, *9*, 4797.

(107) Qiu, L.; Chakraborty, C.; Dhara, S.; Vamivakas, A. N. Room-Temperature Valley Coherence in a Polaritonic System. *Nat. Commun.* **2019**, *10*, 1513.

(108) Lundt, N.; Dusanowski, L.; Sedov, E.; Stepanov, P.; Glazov, M. M.; Klempt, S.; Klaas, M.; Beierlein, J.; Qin, Y.; Tongay, S.; Richard, M.; Kavokin, A. V.; Höfling, S.; Schneider, C. Optical Valley Hall Effect for Highly Valley-Coherent Exciton-Polaritons in an Atomically Thin Semiconductor. *Nat. Nanotechnol.* **2019**, *14*, 770–775.

(109) LaMountain, T.; Nelson, J.; Lenferink, E. J.; Amsterdam, S. H.; Murthy, A. A.; Zeng, H.; Marks, T. J.; Dravid, V. P.; Hersam, M. C.; Stern, N. P. Valley-Selective Optical Stark Effect of Exciton-Polaritons in a Monolayer Semiconductor. *Nat. Commun.* **2021**, *12*, 4530.

(110) Lyons, T. P.; Gillard, D. J.; Leblanc, C.; Puebla, J.; Solnyshkov, D. D.; Klompaker, L.; Akimov, I. A.; Louca, C.; Muduli, P.; Genco, A.; Bayer, M.; Otani, Y.; Malpuech, G.; Tartakovskii, A. I. Giant Effective Zeeman Splitting in a Monolayer Semiconductor Realized by Spin-Selective Strong Light-Matter Coupling. *Nat. Photonics* **2022**, *16*, 632–636.

(111) Barachati, F.; Fieramosca, A.; Hafezian, S.; Gu, J.; Chakraborty, B.; Ballarini, D.; Martinu, L.; Menon, V.; Sanvitto, D.; Kéna-Cohen, S. Interacting Polariton Fluids in a Monolayer of Tungsten Disulfide. *Nat. Nanotechnol.* **2018**, *13*, 906–909.

(112) Gu, J.; Walther, V.; Waldecker, L.; Rhodes, D.; Raja, A.; Hone, J. C.; Heinz, T. F.; Kéna-cohen, S.; Pohl, T.; Menon, V. M. Enhanced

Nonlinear Interaction of Polaritons via Excitonic Rydberg States in Monolayer WSe<sub>2</sub>. *Nat. Commun.* **2021**, *12*, 2269.

(113) Zhang, L.; Wu, F.; Hou, S.; Zhang, Z.; Chou, Y.-H.; Watanabe, K.; Taniguchi, T.; Forrest, S. R.; Deng, H. Van Der Waals Heterostructure Polaritons with Moiré-Induced Nonlinearity. *Nature* **2021**, *591*, 61–65.

(114) Zhao, J.; Fieramosca, A.; Bao, R.; Du, W.; Dini, K.; Su, R.; Feng, J.; Luo, Y.; Sanvitto, D.; Liew, T. C. H.; Xiong, Q. Nonlinear Polariton Parametric Emission in an Atomically Thin Semiconductor Based Microcavity. *Nat. Nanotechnol.* **2022**, *17*, 396–402.

(115) Cilibrizzi, P.; Liu, X.; Zhang, P.; Wang, C.; Li, Q.; Yang, S.; Zhang, X. Self-Induced Valley Bosonic Stimulation of Exciton Polaritons in a Monolayer Semiconductor. *Phys. Rev. Lett.* **2023**, *130*, 36902.

(116) Anton-Solanas, C.; Waldherr, M.; Klaas, M.; Suchomel, H.; Harder, T. H.; Cai, H.; Sedov, E.; Klembt, S.; Kavokin, A. V.; Tongay, S.; Watanabe, K.; Taniguchi, T.; Hofling, S.; Schneider, C. Bosonic Condensation of Exciton-Polaritons in an Atomically Thin Crystal. *Nat. Mater.* **2021**, *20*, 1233–1239.

(117) Zhao, J.; Su, R.; Fieramosca, A.; Zhao, W.; Du, W.; Liu, X.; Diederichs, C.; Sanvitto, D.; Liew, T. C. H.; Xiong, Q. Ultralow Threshold Polariton Condensate in a Monolayer Semiconductor Microcavity at Room Temperature. *Nano Lett.* **2021**, *21*, 3331–3339.

(118) Polimeno, L.; Lerario, G.; De Giorgi, M.; De Marco, L.; Dominici, L.; Todisco, F.; Coriolano, A.; Ardizzone, V.; Pugliese, M.; Prontera, C. T.; Maiorano, V.; Moliterni, A.; Giannini, C.; Olieric, V.; Gigli, G.; Ballarini, D.; Xiong, Q.; Fieramosca, A.; Solnyshkov, D. D.; Malpuech, G.; Sanvitto, D. Tuning of the Berry Curvature in 2D Perovskite Polaritons. *Nat. Nanotechnol.* **2021**, *16*, 1349–1354.

(119) Mak, K. F.; Shan, J. Photonics and Optoelectronics of 2D Semiconductor Transition Metal Dichalcogenides. *Nat. Photonics* **2016**, *10*, 216–226.

(120) Chhowalla, M.; Shin, H. S.; Eda, G.; Li, L.-J.; Loh, K. P.; Zhang, H. The Chemistry of Two-Dimensional Layered Transition Metal Dichalcogenide Nanosheets. *Nat. Chem.* **2013**, *5*, 263–275.

(121) Wang, Q. H.; Kalantar-Zadeh, K.; Kis, A.; Coleman, J. N.; Strano, M. S. Electronics and Optoelectronics of Two-Dimensional Transition Metal Dichalcogenides. *Nat. Nanotechnol.* **2012**, *7*, 699–712.

(122) Cao, T.; Wang, G.; Han, W.; Ye, H.; Zhu, C.; Shi, J.; Niu, Q.; Tan, P.; Wang, E.; Liu, B.; Feng, J. Valley-Selective Circular Dichroism of Monolayer Molybdenum Disulfide. *Nat. Commun.* **2012**, *3*, 887.

(123) Zeng, H.; Dai, J.; Yao, W.; Xiao, D.; Cui, X. Valley Polarization in MoS<sub>2</sub> Monolayers by Optical Pumping. *Nat. Nanotechnol.* **2012**, *7*, 490–493.

(124) Mak, K. F.; He, K.; Shan, J.; Heinz, T. F. Control of Valley Polarization in Monolayer MoS<sub>2</sub> by Optical Helicity. *Nat. Nanotechnol.* **2012**, *7*, 494–498.

(125) Xu, X.; Yao, W.; Xiao, D.; Heinz, T. Spin and Pseudospins in Layered Transition Metal Dichalcogenides. *Nat. Phys.* **2014**, *10*, 343–350.

(126) Zhang, X.-X.; You, Y.; Zhao, S. Y. F.; Heinz, T. F. Experimental Evidence for Dark Excitons in Monolayer WSe<sub>2</sub>. *Phys. Rev. Lett.* **2015**, *115*, No. 257403.

(127) Zhang, X.-X.; Cao, T.; Lu, Z.; Lin, Y.-C.; Zhang, F.; Wang, Y.; Li, Z.; Hone, J. C.; Robinson, J. A.; Smirnov, D.; Louie, S. G.; Heinz, T. F. Magnetic Brightening and Control of Dark Excitons in Monolayer WSe<sub>2</sub>. *Nat. Nanotechnol.* **2017**, *12*, 883–888.

(128) Zhou, Y.; Scuri, G.; Wild, D. S.; High, A. A.; Dibos, A.; Jauregui, L. A.; Shu, C.; De Greve, K.; Pistunova, K.; Joe, A.; Taniguchi, T.; Watanabe, K.; Kim, P.; Lukin, M. D.; Park, H. Probing Dark Excitons in Atomically Thin Semiconductors via Near-Field Coupling to Surface Plasmon Polaritons. *Nat. Nanotechnol.* **2017**, *12*, 856–860.

(129) Wang, G.; Robert, C.; Glazov, M. M.; Cadiz, F.; Courtade, E.; Amand, T.; Lagarde, D.; Taniguchi, T.; Watanabe, K.; Urbaszek, B.; Marie, X. In-Plane Propagation of Light in Transition Metal

Dichalcogenide Monolayers: Optical Selection Rules. *Phys. Rev. Lett.* **2017**, *119*, No. 047401.

(130) Park, K. D.; Jiang, T.; Clark, G.; Xu, X.; Raschke, M. B. Radiative Control of Dark Excitons at Room Temperature by Nano-Optical Antenna-Tip Purcell Effect. *Nat. Nanotechnol.* **2018**, *13*, 59–64.

(131) Ross, J. S.; Wu, S.; Yu, H.; Ghimire, N. J.; Jones, A. M.; Aivazian, G.; Yan, J.; Mandrus, D. G.; Xiao, D.; Yao, W.; Xu, X. Electrical Control of Neutral and Charged Excitons in a Monolayer Semiconductor. *Nat. Commun.* **2013**, *4*, 1474.

(132) You, Y.; Zhang, X. X.; Berkelbach, T. C.; Hybertsen, M. S.; Reichman, D. R.; Heinz, T. F. Observation of Biexcitons in Monolayer WSe<sub>2</sub>. *Nat. Phys.* **2015**, *11*, 477–481.

(133) Ye, Z.; Waldecker, L.; Ma, E. Y.; Rhodes, D.; Antony, A.; Kim, B.; Zhang, X. X.; Deng, M.; Jiang, Y.; Lu, Z.; Smirnov, D.; Watanabe, K.; Taniguchi, T.; Hone, J.; Heinz, T. F. Efficient Generation of Neutral and Charged Biexcitons in Encapsulated WSe<sub>2</sub> Monolayers. *Nat. Commun.* **2018**, *9*, 3718.

(134) Stevens, C. E.; Paul, J.; Cox, T.; Sahoo, P. K.; Gutiérrez, H. R.; Turkowski, V.; Semenov, D.; McGill, S. A.; Kapetanakis, M. D.; Perakis, I. E.; Hilton, D. J.; Karaickaj, D. Biexcitons in Monolayer Transition Metal Dichalcogenides Tuned by Magnetic Fields. *Nat. Commun.* **2018**, *9*, 3720.

(135) Steinhoff, A.; Florian, M.; Singh, A.; Tran, K.; Kolarczik, M.; Helmrich, S.; Achtstein, A. W.; Woggon, U.; Owschimikow, N.; Jahnke, F.; Li, X. Biexciton Fine Structure in Monolayer Transition Metal Dichalcogenides. *Nat. Phys.* **2018**, *14*, 1199–1204.

(136) Barbone, M.; Montblanch, A. R.-P.; Kara, D. M.; Palacios-Berraquero, C.; Cadore, A. R.; De Fazio, D.; Pingault, B.; Mostaani, E.; Li, H.; Chen, B.; Watanabe, K.; Taniguchi, T.; Tongay, S.; Wang, G.; Ferrari, A. C.; Atatüre, M. Charge-Tuneable Biexciton Complexes in Monolayer WSe<sub>2</sub>. *Nat. Commun.* **2018**, *9*, 3721.

(137) Aslan, B.; Chenet, D. A.; Van Der Zande, A. M.; Hone, J. C.; Heinz, T. F. Linearly Polarized Excitons in Single- and Few-Layer ReS<sub>2</sub> Crystals. *ACS Photonics* **2016**, *3*, 96–101.

(138) Low, T.; Chaves, A.; Caldwell, J. D.; Kumar, A.; Fang, N. X.; Avouris, P.; Heinz, T. F.; Guinea, F.; Martin-Moreno, L.; Koppens, F. Polaritons in Layered Two-Dimensional Materials. *Nat. Mater.* **2017**, *16*, 182–194.

(139) Gogna, R.; Zhang, L.; Deng, H. Self-Hybridized, Polarized Polaritons in ReS<sub>2</sub> Crystals. *ACS Photonics* **2020**, *7*, 3328–3332.

(140) Chakrabarty, D.; Dhara, A.; Ghosh, K.; Pattanayak, A. K.; Mukherjee, S.; Chaudhuri, A. R.; Dhara, S. Interfacial Anisotropic Exciton-Polariton Manifolds in ReS<sub>2</sub>. *Optica* **2021**, *8*, 1488.

(141) Coriolano, A.; Polimeno, L.; Pugliese, M.; Cannavale, A.; Trypogeorgos, D.; Di Renzo, A.; Ardizzone, V.; Rizzo, A.; Ballarini, D.; Gigli, G.; Maiorano, V.; Rosyadi, A. S.; Chuang, C.-A.; Ho, C.-H.; De Marco, L.; Sanvitto, D.; De Giorgi, M. Rydberg Polaritons in ReS<sub>2</sub> Crystals. *Sci. Adv.* **2022**, *8*, No. eadd8857.

(142) Paradisanos, I.; Urbaszek, B. Excitons Dance as Light Conducts. *Nat. Phys.* **2023**, *19*, 149.

(143) Rivera, P.; Yu, H.; Seyler, K. L.; Wilson, N. P.; Yao, W.; Xu, X. Interlayer Valley Excitons in Heterobilayers of Transition Metal Dichalcogenides. *Nat. Nanotechnol.* **2018**, *13*, 1004–1015.

(144) Regan, E. C.; Wang, D.; Paik, E. Y.; Zeng, Y.; Zhang, L.; Zhu, J.; MacDonald, A. H.; Deng, H.; Wang, F. Emerging Exciton Physics in Transition Metal Dichalcogenide Heterobilayers. *Nat. Rev. Mater.* **2022**, *7*, 778–795.

(145) Du, L.; Molas, M. R.; Huang, Z.; Zhang, G.; Wang, F.; Sun, Z. Moiré Photonics and Optoelectronics. *Science* **2023**, *379*, No. eadg0014.

(146) Rivera, P.; Seyler, K. L.; Yu, H.; Schaibley, J. R.; Yan, J.; Mandrus, D. G.; Yao, W.; Xu, X. Valley-Polarized Exciton Dynamics in a 2D Semiconductor Heterostructure. *Science* **2016**, *351*, 688–691.

(147) Barré, E.; Karni, O.; Liu, E.; O’Beirne, A. L.; Chen, X.; Ribeiro, H. B.; Yu, L.; Kim, B.; Watanabe, K.; Taniguchi, T.; Barmak, K.; Lui, C. H.; Refaely-Abramson, S.; da Jornada, F. H.; Heinz, T. F. Optical Absorption of Interlayer Excitons in Transition-Metal Dichalcogenide Heterostructures. *Science* **2022**, *376*, 406–410.

- (148) Tang, Y.; Gu, J.; Liu, S.; Watanabe, K.; Taniguchi, T.; Hone, J.; Mak, K. F.; Shan, J. Tuning Layer-Hybridized Moiré Excitons by the Quantum-Confined Stark Effect. *Nat. Nanotechnol.* **2021**, *16*, 52–57.
- (149) Leisgang, N.; Shree, S.; Paradisanos, I.; Sponfeldner, L.; Robert, C.; Lagarde, D.; Balocchi, A.; Watanabe, K.; Taniguchi, T.; Marie, X.; Warburton, R. J.; Gerber, I. C.; Urbaszek, B. Giant Stark Splitting of an Exciton in Bilayer MoS<sub>2</sub>. *Nat. Nanotechnol.* **2020**, *15*, 901–907.
- (150) Alexeev, E. M.; Ruiz-Tijerina, D. A.; Danovich, M.; Hamer, M. J.; Terry, D. J.; Nayak, P. K.; Ahn, S.; Pak, S.; Lee, J.; Sohn, J. I.; Molas, M. R.; Koperski, M.; Watanabe, K.; Taniguchi, T.; Novoselov, K. S.; Gorbachev, R. V.; Shin, H. S.; Fal'ko, V. I.; Tartakovskii, A. I. Resonantly Hybridized Excitons in Moiré Superlattices in van Der Waals Heterostructures. *Nature* **2019**, *567*, 81–86.
- (151) Zhang, L.; Zhang, Z.; Wu, F.; Wang, D.; Gogna, R.; Hou, S.; Watanabe, K.; Taniguchi, T.; Kulkarni, K.; Kuo, T.; Forrest, S. R.; Deng, H. Twist-Angle Dependence of Moiré Excitons in WS<sub>2</sub>/MoSe<sub>2</sub> Heterobilayers. *Nat. Commun.* **2020**, *11*, 5888.
- (152) Seyler, K. L.; Rivera, P.; Yu, H.; Wilson, N. P.; Ray, E. L.; Mandrus, D.; Yan, J.; Yao, W.; Xu, X. Signatures of Moiré Trapped Valley Excitons in MoSe<sub>2</sub>/WSe<sub>2</sub> Heterobilayers. *Nature* **2019**, *567*, 66–70.
- (153) Shimazaki, Y.; Schwartz, I.; Watanabe, K.; Taniguchi, T.; Kroner, M.; Imamoğlu, A. Strongly Correlated Electrons and Hybrid Excitons in a Moiré Heterostructure. *Nature* **2020**, *580*, 472–477.
- (154) Jin, C.; Regan, E. C.; Yan, A.; Iqbal Bakti Utama, M.; Wang, D.; Zhao, S.; Qin, Y.; Yang, S.; Zheng, Z.; Shi, S.; Watanabe, K.; Taniguchi, T.; Tongay, S.; Zettl, A.; Wang, F. Observation of Moiré Excitons in WSe<sub>2</sub>/WS<sub>2</sub> Heterostructure Superlattices. *Nature* **2019**, *567*, 76–80.
- (155) Tran, K.; Moody, G.; Wu, F.; Lu, X.; Choi, J.; Kim, K.; Rai, A.; Sanchez, D. A.; Quan, J.; Singh, A.; Embley, J.; Zepeda, A.; Campbell, M.; Autry, T.; Taniguchi, T.; Watanabe, K.; Lu, N.; Banerjee, S. K.; Silverman, K. L.; Kim, S.; Tutuc, E.; Yang, L.; MacDonald, A. H.; Li, X. Evidence for Moiré Excitons in van Der Waals Heterostructures. *Nature* **2019**, *567*, 71–75.
- (156) Wu, F.; Lovorn, T.; Macdonald, A. H. Topological Exciton Bands in Moiré Heterojunctions. *Phys. Rev. Lett.* **2017**, *118*, No. 147401.
- (157) Yu, H.; Liu, G.; Tang, J.; Xu, X.; Yao, W. Moiré Excitons: From Programmable Quantum Emitter Arrays to Spin-Orbit – Coupled Artificial Lattices. *Sci. Adv.* **2017**, *3*, No. e1701696.
- (158) Dufferwiel, S.; Schwarz, S.; Withers, F.; Trichet, A. A. P.; Li, F.; Sich, M.; Del Pozo-Zamudio, O.; Clark, C.; Nalitov, A.; Solnyshkov, D. D.; Malpuech, G.; Novoselov, K. S.; Smith, J. M.; Skolnick, M. S.; Krizhanovskii, D. N.; Tartakovskii, A. I. Exciton–Polaritons in van Der Waals Heterostructures Embedded in Tunable Microcavities. *Nat. Commun.* **2015**, *6*, 8579.
- (159) Flatten, L. C.; He, Z.; Coles, D. M.; Trichet, A. A. P.; Powell, A. W.; Taylor, R. A.; Warner, J. H.; Smith, J. M. Room-Temperature Exciton-Polaritons with Two-Dimensional WS<sub>2</sub>. *Sci. Rep.* **2016**, *6*, 33134.
- (160) Munkhbat, B.; Canales, A.; Kucukoz, B.; Baranov, D. G.; Shegai, T. Tunable Self-Assembled Casimir Microcavities and Polaritons. *Nature* **2021**, *597*, 214–219.
- (161) Chakraborty, B.; Gu, J.; Sun, Z.; Khatoniar, M.; Bushati, R.; Boehmke, A. L.; Koots, R.; Menon, V. M. Control of Strong Light–Matter Interaction in Monolayer WS<sub>2</sub> through Electric Field Gating. *Nano Lett.* **2018**, *18*, 6455–6460.
- (162) Dhara, S.; Chakraborty, C.; Goodfellow, K. M.; Qiu, L.; O'Loughlin, T. A.; Wicks, G. W.; Bhattacharjee, S.; Vamivakas, A. N. Anomalous Dispersion of Microcavity Trion-Polaritons. *Nat. Phys.* **2018**, *14*, 130–133.
- (163) Sidler, M.; Back, P.; Cotlet, O.; Srivastava, A.; Fink, T.; Kroner, M.; Demler, E.; Imamoğlu, A. Fermi Polaron-Polaritons in Charge-Tunable Atomically Thin Semiconductors. *Nat. Phys.* **2017**, *13*, 255–261.
- (164) Kyriienko, O.; Krizhanovskii, D. N.; Shelykh, I. A. Nonlinear Quantum Optics with Trion Polaritons in 2D Monolayers: Conventional and Unconventional Photon Blockade. *Phys. Rev. Lett.* **2020**, *125*, No. 197402.
- (165) Rana, F.; Koksai, O.; Jung, M.; Shvets, G.; Vamivakas, A. N.; Manolatu, C. Exciton-Trion Polaritons in Doped Two-Dimensional Semiconductors. *Phys. Rev. Lett.* **2021**, *126*, No. 127402.
- (166) Emmanuele, R. P. A.; Sich, M.; Kyriienko, O.; Shahnazaryan, V.; Withers, F.; Catanzaro, A.; Walker, P. M.; Benimetskiy, F. A.; Skolnick, M. S.; Tartakovskii, A. I.; Shelykh, I. A.; Krizhanovskii, D. N. Highly Nonlinear Trion-Polaritons in a Monolayer Semiconductor. *Nat. Commun.* **2020**, *11*, 3589.
- (167) Kleemann, M. E.; Chikkaraddy, R.; Alexeev, E. M.; Kos, D.; Carnegie, C.; Deacon, W.; De Pury, A. C.; Große, C.; De Nijs, B.; Mertens, J.; Tartakovskii, A. I.; Baumberg, J. J. Strong-Coupling of WSe<sub>2</sub> in Ultra-Compact Plasmonic Nanocavities at Room Temperature. *Nat. Commun.* **2017**, *8*, 1296.
- (168) Lee, B.; Park, J.; Han, G. H.; Ee, H. S.; Naylor, C. H.; Liu, W.; Johnson, A. T. C.; Agarwal, R. Fano Resonance and Spectrally Modified Photoluminescence Enhancement in Monolayer MoS<sub>2</sub> Integrated with Plasmonic Nanoantenna Array. *Nano Lett.* **2015**, *15*, 3646–3653.
- (169) Wen, J.; Wang, H.; Wang, W.; Deng, Z.; Zhuang, C.; Zhang, Y.; Liu, F.; She, J.; Chen, J.; Chen, H.; Deng, S.; Xu, N. Room-temperature Strong Light-Matter Interaction with Active Control in Single Plasmonic Nanorod Coupled with Two-Dimensional Atomic Crystals. *Nano Lett.* **2017**, *17*, 4689–4697.
- (170) Zheng, D.; Zhang, S.; Deng, Q.; Kang, M.; Nordlander, P.; Xu, H. Manipulating Coherent Plasmon-Exciton Interaction in a Single Silver Nanorod on Monolayer WSe<sub>2</sub>. *Nano Lett.* **2017**, *17*, 3809–3814.
- (171) Cuadra, J.; Baranov, D. G.; Wersäll, M.; Verre, R.; Antosiewicz, T. J.; Shegai, T. Observation of Tunable Charged Exciton Polaritons in Hybrid Monolayer WS<sub>2</sub> – Plasmonic Nanoantenna System. *Nano Lett.* **2018**, *18*, 1777–1785.
- (172) Qin, J.; Chen, Y.-H.; Zhang, Z.; Zhang, Y.; Blaikie, R. J.; Ding, B.; Qiu, M. Revealing Strong Plasmon-Exciton Coupling between Nanogap Resonators and Two-Dimensional Semiconductors at Ambient Conditions. *Phys. Rev. Lett.* **2020**, *124*, No. 063902.
- (173) Liu, X.; Yi, J.; Yang, S.; Lin, E.-C.; Zhang, Y.-J.; Zhang, P.; Li, J.-F.; Wang, Y.; Lee, Y.-H.; Tian, Z.-Q.; Zhang, X. Nonlinear Valley Phonon Scattering under the Strong Coupling Regime. *Nat. Mater.* **2021**, *20*, 1210–1215.
- (174) Niu, Y.; Xu, H.; Wei, H. Unified Scattering and Photoluminescence Spectra for Strong Plasmon-Exciton Coupling. *Phys. Rev. Lett.* **2022**, *128*, No. 167402.
- (175) Datta, B.; Khatoniar, M.; Deshmukh, P.; Thouin, F.; Bushati, R.; De Liberato, S.; Cohen, S. K.; Menon, V. M. Highly Non-Linear Interlayer Exciton-Polaritons in Bilayer MoS<sub>2</sub>. *Nat. Commun.* **2022**, *13*, 6341.
- (176) Mak, K. F.; Shan, J. Semiconductor Moiré Materials. *Nat. Nanotechnol.* **2022**, *17*, 686–695.
- (177) Al-Ani, I. A. M.; As'Ham, K.; Huang, L.; Miroshnichenko, A. E.; Hattori, H. T. Enhanced Strong Coupling of TMDC Monolayers by Bound State in the Continuum. *Laser Photonics Rev.* **2021**, *15*, 1–11.
- (178) Saba, M.; Ciuti, C.; Bloch, J.; Thierry-Mieg, V.; Andre, R.; Dang, L. S.; Kundermann, S.; Mura, A.; Bongiovanni, G.; Staehli, J. L.; Deveaud, B. High-Temperature Ultrafast Polariton Parametric Amplification in Semiconductor Microcavities. *Nature* **2001**, *414*, 731–735.
- (179) Lundt, N.; Klaas, M.; Sedov, E.; Waldherr, M.; Knopf, H.; Blei, M.; Tongay, S.; Klembt, S.; Taniguchi, T.; Watanabe, K.; Schulz, U.; Kavokin, A.; Höfling, S.; Eilenberger, F.; Schneider, C. Magnetic-Field-Induced Splitting and Polarization of Monolayer-Based Valley Exciton Polaritons. *Phys. Rev. B* **2019**, *100*, No. 121303(R).
- (180) Shan, H.; Lackner, L.; Han, B.; Sedov, E.; Rupprecht, C.; Knopf, H.; Eilenberger, F.; Beierlein, J.; Kunte, N.; Esmann, M.; Yumigeta, K.; Watanabe, K.; Taniguchi, T.; Klembt, S.; Höfling, S.;

- Kavokin, A. V.; Tongay, S.; Schneider, C.; Anton-Solanas, C. Spatial Coherence of Room-Temperature Monolayer WSe<sub>2</sub> Exciton-Polaritons in a Trap. *Nat. Commun.* **2021**, *12*, 6406.
- (181) Jones, A. M.; Yu, H.; Ghimire, N. J.; Wu, S.; Aivazian, G.; Ross, J. S.; Zhao, B.; Yan, J.; Mandrus, D. G.; Xiao, D.; Yao, W.; Xu, X. Optical Generation of Excitonic Valley Coherence in Monolayer WSe<sub>2</sub>. *Nat. Nanotechnol.* **2013**, *8*, 634–648.
- (182) Qiu, L.; Chakraborty, C.; Dhara, S.; Vamivakas, A. N. Room-Temperature Valley Coherence in a Polaritonic System. *Nat. Commun.* **2019**, *10*, 1513.
- (183) Yao, W.; Xiao, D.; Niu, Q. Valley-Dependent Optoelectronics from Inversion Symmetry Breaking. *Phys. Rev. B* **2008**, *77*, No. 235406.
- (184) Mak, K. F.; McGill, K. L.; Park, J.; Mceuen, P. L. The Valley Hall Effect in MoS<sub>2</sub> Transistors. *Science* **2014**, *344*, 1489–1492.
- (185) Schaibley, J. R.; Yu, H.; Clark, G.; Rivera, P.; Ross, J. S.; Seyler, K. L.; Yao, W.; Xu, X. Valleytronics in 2D Materials. *Nat. Rev. Mater.* **2016**, *1*, 16055.
- (186) Onga, M.; Zhang, Y.; Ideue, T.; Iwasa, Y. Exciton Hall Effect and Transport of Valley Exciton in Monolayer MoS<sub>2</sub>. *Nat. Mater.* **2017**, *16*, 1193.
- (187) Kim, N. Y.; Nitsche, W. H.; Yamamoto, Y. Berezinskii-Kosterlitz-Thouless Phase of a Driven-Dissipative Condensate. In *Universal Themes of Bose–Einstein Condensation*; Proukakis, N. P., Snoke, D. W., Littlewood, P. B., Eds.; Cambridge University Press, 2017; pp 187–204.
- (188) Savvidis, P. G.; Baumberg, J. J.; Stevenson, R. M.; Skolnick, M. S.; Whittaker, D. M.; Roberts, J. S. Angle-Resonant Stimulated Polariton Amplifier. *Phys. Rev. Lett.* **2000**, *84*, 1547–1550.
- (189) Gu, J.; Chakraborty, B.; Khatoniar, M.; Menon, V. M. A Room-Temperature Polariton Light-Emitting Diode Based on Monolayer WS<sub>2</sub>. *Nat. Nanotechnol.* **2019**, *14*, 1024–1028.
- (190) Zhao, J.; Fieramosca, A.; Dini, K.; Bao, R.; Du, W.; Su, R.; Luo, Y.; Zhao, W.; Sanvitto, D.; Liew, T. C. H.; Xiong, Q. Exciton Polariton Interactions in Van Der Waals Superlattices at Room Temperature. *Nat. Commun.* **2023**, *14*, 1512.
- (191) Kazimierczuk, T.; Fröhlich, D.; Scheel, S.; Stolz, H.; Bayer, M. Giant Rydberg Excitons in the Copper Oxide Cu<sub>2</sub>O. *Nature* **2014**, *514*, 343–347.
- (192) Wang, J.; Su, R.; Xing, J.; Bao, D.; Diederichs, C.; Liu, S.; Liew, T. C. H.; Chen, Z.; Xiong, Q. Room Temperature Coherently Coupled Exciton–Polaritons in Two-Dimensional Organic–Inorganic Perovskite. *ACS Nano* **2018**, *12*, 8382–8389.
- (193) Polimeno, L.; Fieramosca, A.; Lerario, G.; Cinguino, M.; De Giorgi, M.; Ballarini, D.; Todisco, F.; Dominici, L.; Ardizzone, V.; Pugliese, M.; Prontera, C. T.; Maiorano, V.; Gigli, G.; De Marco, L.; Sanvitto, D. Observation of Two Thresholds Leading to Polariton Condensation in 2D Hybrid Perovskites. *Adv. Opt. Mater.* **2020**, *8*, No. 2000176.
- (194) Lempicka-Mirek, K.; Król, M.; Sigurdsson, H.; Wincukiewicz, A.; Morawiak, P.; Mazur, R.; Muszyński, M.; Piecek, W.; Kula, P.; Stefaniuk, T.; Kamińska, M.; De Marco, L.; Lagoudakis, P. G.; Ballarini, D.; Sanvitto, D.; Szczytko, J.; Piętko, B. Electrically Tunable Berry Curvature and Strong Light-Matter Coupling in Liquid Crystal Microcavities with 2D Perovskite. *Sci. Adv.* **2022**, *8*, No. eabq7533.
- (195) Spencer, M. S.; Fu, Y.; Schlaus, A. P.; Hwang, D.; Dai, Y.; Smith, M. D.; Gamelin, D. R.; Zhu, X.-Y. Spin-Orbit–Coupled Exciton-Polariton Condensates in Lead Halide Perovskites. *Sci. Adv.* **2021**, *7*, No. eabj7667.
- (196) Peng, K.; Tao, R.; Haeberlé, L.; Li, Q.; Jin, D.; Fleming, G. R.; Kéna-Cohen, S.; Zhang, X.; Bao, W. Room-Temperature Polariton Quantum Fluids in Halide Perovskites. *Nat. Commun.* **2022**, *13*, 7388.
- (197) Ren, J.; Liao, Q.; Li, F.; Li, Y.; Bleu, O.; Malpuech, G.; Yao, J.; Fu, H.; Solnyshkov, D. Nontrivial Band Geometry in an Optically Active System. *Nat. Commun.* **2021**, *12*, 689.
- (198) Diederich, G. M.; Cenker, J.; Ren, Y.; Fonseca, J.; Chica, D. G.; Bae, Y. J.; Zhu, X.; Roy, X.; Cao, T.; Xiao, D.; Xu, X. Tunable Interaction between Excitons and Hybridized Magnons in a Layered Semiconductor. *Nat. Nanotechnol.* **2023**, *18*, 23–28.
- (199) Huang, B.; Clark, G.; Navarro-Moratalla, E.; Klein, D. R.; Cheng, R.; Seyler, K. L.; Zhong, D.; Schmidgall, E.; McGuire, M. A.; Cobden, D. H.; Yao, W.; Xiao, D.; Jarillo-Herrero, P.; Xu, X. Layer-Dependent Ferromagnetism in a van Der Waals Crystal down to the Monolayer Limit. *Nature* **2017**, *546*, 270–273.
- (200) Gong, C.; Li, L.; Li, Z.; Ji, H.; Stern, A.; Xia, Y.; Cao, T.; Bao, W.; Wang, C.; Wang, Y.; Qiu, Z. Q.; Cava, R. J.; Louie, S. G.; Xia, J.; Zhang, X. Discovery of Intrinsic Ferromagnetism in Two-Dimensional van Der Waals Crystals. *Nature* **2017**, *546*, 265–269.
- (201) Gong, C.; Zhang, X. Two-Dimensional Magnetic Crystals and Emergent Heterostructure Devices. *Science* **2019**, *363*, No. eaav4450.
- (202) Bae, Y. J.; Wang, J.; Scheie, A.; Xu, J.; Chica, D. G.; Diederich, G. M.; Cenker, J.; Ziebel, M. E.; Bai, Y.; Ren, H.; Dean, C. R.; Delor, M.; Xu, X.; Roy, X.; Kent, A. D.; Zhu, X. Exciton-Coupled Coherent Magnons in a 2D Semiconductor. *Nature* **2022**, *609*, 282–286.
- (203) Hwangbo, K.; Zhang, Q.; Jiang, Q.; Wang, Y.; Fonseca, J.; Wang, C.; Diederich, G. M.; Gamelin, D. R.; Xiao, D.; Chu, J.-H.; Yao, W.; Xu, X. Highly Anisotropic Excitons and Multiple Phonon Bound States in a van Der Waals Antiferromagnetic Insulator. *Nat. Nanotechnol.* **2021**, *16*, 655–660.
- (204) Wang, X.; Cao, J.; Lu, Z.; Cohen, A.; Kitadai, H.; Li, T.; Tan, Q.; Wilson, M.; Lui, C. H.; Smirnov, D.; Sharifzadeh, S.; Ling, X. Spin-Induced Linear Polarization of Photoluminescence in Antiferromagnetic van Der Waals Crystals. *Nat. Mater.* **2021**, *20*, 964–970.
- (205) Su, R.; Ghosh, S.; Wang, J.; Liu, S.; Diederichs, C.; Liew, T. C. H.; Xiong, Q. Observation of Exciton Polariton Condensation in a Perovskite Lattice at Room Temperature. *Nat. Phys.* **2020**, *16*, 301–306.
- (206) Liu, A.; Guan, G.; Chai, X.; Feng, N.; Lu, M.; Bai, X.; Zhang, Y. Metal Halide Perovskites toward Electrically Pumped Lasers. *Laser Photonics Rev.* **2022**, *16*, No. 2200189.
- (207) Shalae, M. I.; Walasik, W.; Tsukernik, A.; Xu, Y.; Litchinitser, N. M. Robust Topologically Protected Transport in Photonic Crystals at Telecommunication Wavelengths. *Nat. Nanotechnol.* **2019**, *14*, 31–34.
- (208) He, X.-T.; Liang, E.-T.; Yuan, J.-J.; Qiu, H.-Y.; Chen, X.-D.; Zhao, F.-L.; Dong, J.-W. A Silicon-on-Insulator Slab for Topological Valley Transport. *Nat. Commun.* **2019**, *10*, 872.
- (209) Wu, J.; Ghosh, S.; Gan, Y.; Shi, Y.; Mandal, S.; Sun, H.; Zhang, B.; Liew, T. C. H.; Su, R.; Xiong, Q. Higher-Order Topological Polariton Corner State Lasing. *Sci. Adv.* **2023**, *9*, No. eadg4322.
- (210) Gao, X.; Yang, L.; Lin, H.; Zhang, L.; Li, J.; Bo, F.; Wang, Z.; Lu, L. Dirac-Vortex Topological Cavities. *Nat. Nanotechnol.* **2020**, *15*, 1012–1018.
- (211) Ma, J.; Xi, X.; Li, Y.; Sun, X. Nanomechanical Topological Insulators with an Auxiliary Orbital Degree of Freedom. *Nat. Nanotechnol.* **2021**, *16*, 576–583.
- (212) Pernet, N.; St-Jean, P.; Solnyshkov, D. D.; Malpuech, G.; Carlon Zambon, N.; Fontaine, Q.; Real, B.; Jamadi, O.; Lemaître, A.; Morassi, M.; Le Gratiet, L.; Baptiste, T.; Harouri, A.; Sagnes, I.; Amo, A.; Ravets, S.; Bloch, J. Gap Solitons in a One-Dimensional Driven-Dissipative Topological Lattice. *Nat. Phys.* **2022**, *18*, 678–684.
- (213) Isakov, S. V.; Hastings, M. B.; Melko, R. G. Topological Entanglement Entropy of a Bose–Hubbard Spin Liquid. *Nat. Phys.* **2011**, *7*, 772–775.